TECHNICAL MEMORANDUM

804

Assessment of the forecast impact of surface-sensitive microwave radiances over land and sea-ice

Niels Bormann, Cristina Lupu, Alan Geer, Heather Lawrence, Peter Weston and Stephen English

Research Department

October 2017

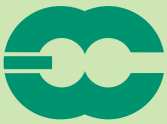

European Centre for Medium-Range Weather Forecasts
Europäisches Zentrum für mittelfristige Wettervorhersage
Centre européen pour les prévisions météorologiques à moyen terme

Series: ECMWF Technical Memoranda

A full list of ECMWF Publications can be found on our web site under:
http://www.ecmwf.int/en/research/publications

Contact: library@ecmwf.int

European Centre for Medium-Range Weather Forecasts
Shinfield Park, Reading, RG2 9AX, England

Abstract

The present forecast impact of surface-sensitive microwave sounder radiances over land and sea-ice has been assessed in the ECMWF system, using observing system experiments as well as adjoint-based diagnostics. The assimilation relies on surface emissivities retrieved from window channel observations. Short-comings of the current use of the data in specific regions are also highlighted.

Surface-sensitive microwave radiances over land and sea-ice have a significant positive forecast impact in the ECMWF system (2-3 % reduction in forecast error for the 500 hPa geopotential over the extra-tropics). When added incrementally to an otherwise full observing system, observations over sea-ice, humidity-sounding radiances over land, and temperature-sounding radiances over land all contribute significantly to this positive forecast impact. The impact shows some seasonal dependence, and the Northern Hemisphere impact over land is smaller during winter, most likely related to a more restricted and less optimal use of the observations over snow.

Short-comings are nevertheless apparent in specific areas. Desert regions show diurnal biases, most likely due to biases in the temperature used to specify surface radiation, likely arising from a combination of penetration effects and diurnal model biases. Snow-covered regions show biases that appear consistent with assuming specular reflection when diffuse reflection is prevalent. The quality control currently applied is mostly successful in protecting the analysis from the deficiencies in these areas. Neglected cloud signals can have a significant effect on the retrieved emissivities and the subsequent quality control. Potential avenues to improve the identified short-comings are outlined.

1 Introduction

This memorandum provides an assessment of the impact of surface-sensitive microwave sounding data over land and sea-ice in the ECMWF assimilation system. Data from microwave sounders (e.g., AMSU-A, ATMS, MHS, SSMIS) are leading contributors to today's forecast skill, with tropospheric sounding channels being especially important for reliable weather forecasts. Many of these tropospheric channels exhibit some sensitivity to the surface, and the use of these channels for atmospheric applications is more straightforward over sea. This is because accurate surface emissivity models are available for the relevant frequencies (e.g., Liu et al. 2011), and errors in the skin temperature tend to be relatively small (< 0.5 K), combined with smaller contributions from the surface emission due to a smaller emissivity ($\approx$0.65). In contrast, over land and sea-ice, skin temperature is less well known than over ocean, and this matters more due to larger surface emissivities (0.8-0.95 for most surfaces). In addition, the surface emissivity depends on many more parameters, depending on the surface type, making it harder to model in an operational environment. These larger uncertainties in skin temperature and emissivity hence pose a larger challenge for the assimilation of surface-sensitive data over land and sea-ice regions (e.g., English 2008).

Over the last decade, steady progress has been made regarding the extended data usage over land and sea-ice for microwave sounding data at ECMWF. This has built on methods that retrieve surface emissivity from window channel observations with the help of atmospheric profile and surface temperature information from the First Guess used in the assimilation (Karbou et al 2006, Krzeminski et al. 2008). The method has been applied to temperature as well as humidity-sounding channels, and replaced the previously used parametric models that were based on a broad classification by surface-type (Kelly and Bauer 2000).

The dynamic emissivity retrieval has allowed the gradual extension of the assimilation of surface-sensitive microwave data over land. For instance, the lowest sounding channel from 183 GHz humidity sounders has been added, with some benefits in terms of describing total column water vapour in the analysis (e.g.,

Di Tomaso and Bormann 2012). The method has also been gradually adapted to a wide range of instruments, now covering AMSU-A, ATMS, MHS, and SSMIS (e.g., Lawrence and Bormann 2014, Baordo and Geer 2016). An appropriately chosen emissivity retrieval has allowed the extension of the use of humidity-sounding channels over sea-ice and snow-covered surfaces (e.g., Di Tomaso et al. 2013). The approaches have been successfully transferred to the all-sky use of humidity sounding channels over land and sea-ice (e.g., Baordo and Geer 2016), further increasing data coverage and forecast benefit through the all-sky use (Geer et al. 2017).

Additional refinements of the use of surface-sensitive microwave data over land and sea-ice include the use of scene-dependent observation errors for temperature-sounding channels. This development aims to capture the variable uncertainty in the forward modelling associated with the surface contributions (Lawrence et al. 2015), and down-weights observations for which the uncertainty is larger.

While the impact of each of these separate developments and refinements of the data usage over land and sea-ice on headline forecast scores has been mostly relatively small, we assess here the combined effect and summarise the present impact of surface-sensitive microwave observations over land and sea-ice in the ECMWF system. In this context it is worth pointing out an additional challenge of using satellite observations over land: many land areas (e.g., Europe, North America, China) are of course also well-covered by conventional observations, already providing a good constraint on the analysis. We hence expect benefit from observations over land to originate primarily from remote land or sea-ice areas, and this aspect will also be considered in the assessment.

An additional aim of this paper is to identify strengths and weaknesses of the current data usage, and to point to directions for future development. For instance, we aim to identify whether there are particular geographical regions for which the current approach shows limitations which could be overcome through a refined treatment of the surface contributions. In addition, presently, no attempt is made to actively use the surface information contained in the observations assimilated for the atmospheric analysis (ie, information on surface temperature, or surface conditions). With the development of coupled assimilation approaches, we will also consider the longer-term perspective to outline prospects for an enhanced use of the surface-related information.

The structure of the report is as follows: we first provide an overview of the observation impact experiments performed in this study, followed by a characterisation of the impact demonstrated in these experiments. We will then take a look at adjoint-based observation impact diagnostics, in an attempt to provide further geographical characterisation of the observation impact. Finally, we identify and investigate some issues and short-comings in the present approaches in specific areas and discuss ways forward. A summary and conclusions are provided in the last section.

2 Data usage and experiments

2.1 Data usage over land and sea-ice

The use of surface-sensitive microwave radiances over land and sea-ice in the operational ECMWF system employs the “dynamic emissivity” concept (Karbou et al 2006) to specify an effective surface emissivity for the radiative-transfer calculations (e.g., Krzeminski et al. 2008). The scheme retrieves surface emissivity from observations in a selected window channel that is otherwise not assimilated. This is done by solving the radiative transfer equation for the surface emissivity and estimating the required terms using atmospheric profiles and skin temperature information taken from the model background.

The emissivity estimated from the window channel observation is then used in the radiative transfer calculations for the sounding channels that have similar frequencies. All radiative transfer calculations are assuming specular reflection, for the emissivity retrieval as well as the subsequent assimilation of sounding channels. While this has been found adequate for most surfaces (Karbou et al 2006), it has been put into question, for instance, for snow-covered areas (e.g., Mätzler 2005, Guedj et al. 2010, Baordo and Geer 2015).

The choice of channel for the emissivity estimation involves a trade-off between selecting a channel with good surface sensitivity to allow a reliable emissivity retrieval, and selecting a channel that is sufficiently close in frequency to the sounding channels, to avoid emissivity variations with frequency playing a significant role. For temperature sounding channels in the 50-60 GHz range, emissivity retrieved from the 50.3 GHz channel is used, as this channel provides good surface sensitivity (surface-to-space transmittance τ typically 0.6-0.7) and retrievals at a frequency close to the sounding channels. For 183 GHz humidity sounding channels, we use the emissivity retrieved from the collocated window channel at 89 GHz rather than the closer 150 or 165 GHz channels over most land areas, as it provides better surface sensitivity and less dependence on humidity, and as frequency variations of emissivity are sufficiently small over most surfaces (e.g., Karbou et al 2006). However, over snow and sea-ice areas, where the atmosphere is usually relatively dry and hence sufficiently transparent at 150-165 GHz and frequency dependence matters more, we use the available 150 or 165 GHz channels (e.g., Di Tomaso et al. 2013). An empirical frequency parameterisation is used in this case to obtain an emissivity at 89 GHz in the clear-sky system where this is required for geophysical quality control.

The dynamic emissivity scheme is currently applied to all microwave sounding data assimilated over land and sea-ice in the ECMWF system. Some of these are assimilated in clear-sky conditions only (AMSU-A, ATMS), whereas the majority of the humidity-sensitive observations (MHS, SSMIS) are assimilated in all-sky conditions, that is in clear as well as cloud or rain affected situations (e.g., Geer et al 2014, Baordo and Geer 2016). For the clear-sky assimilation of the microwave temperature-sounding channels, cloud-affected observations over land or sea-ice are screened out by requiring the absolute value of the First Guess (FG)-departure in the 52.8 GHz window channel to be less than 0.7 K. Further cloud detection for AMSU-A channel 5 and 6 (ATMS channels 6 and 7) is performed based on a scatter index, requiring the difference between the 23 GHz and 89 GHz channel to be less than 3 K over surfaces classed as snow-free from the observations. It is important to recognise that the departure check on channel 4 also acts as implicit quality control on the retrieved emissivity and the applied skin temperature: for instance, if the skin temperature is significantly in error (say, by more than 5 K), the skin temperature error will be aliased into the emissivity estimate through the emissivity retrieval at 50.3 GHz, but the departures for the 52.8 GHz channel calculated with this derived emissivity will detect such inconsistencies. A similar check is performed for the 183 GHz channels of ATMS, assimilated in the clear-sky system. These require the departures in the 165 GHz channel to be less than 5 K (over sea-ice, the 89 GHz channel is used instead for this). For the observations in the all-sky system, the retrieved emissivities are compared to values from a climatological emissivity atlas, and retrievals with deviations that are too large by twice the typical standard deviations are replaced by atlas values. This is particularly important in the all-sky system, where mismatched cloud signals from observations or background can lead to larger erroneous emissivity retrievals (Baordo and Geer 2016). No cloud screening is performed in the all-sky system; larger representation errors associated with the presence of clouds in either the observations or the background fields are taken into account by assigning larger observation errors, using as cloud indicator either a scatter index (MHS) or a polarisation difference (SSMIS).

Observational biases are addressed through Variational Bias Correction (VarBC, Dee 2004). The bias model for the sounding radiances uses a global offset combined with four layer thicknesses as linear air-

mass predictors, and it employs a third-order polynomial to model scan-position dependent biases. For channel 4 and 5 of AMSU-A (channels 5, 6 and 17 for ATMS), a separate offset and scan-bias model is used over land and sea-ice, to account for a different bias pattern compared to data over sea (Krzeminski et al. 2008). The different bias pattern most likely reflect differences in the emissivity bias between the FASTEM emissivity model which is used over sea and the dynamic emissivities used over land and sea-ice.

The clear-sky system has two additional features aimed to take into account the larger uncertainty associated with emissivity estimates and the surface temperature over land and sea-ice. Firstly, the surface temperature is treated as a so-called sink variable, that is, one value is retrieved for each satellite sounding during the 4DVAR assimilation. This estimate is discarded and does not affect the subsequent forecast or the next analysis. This skin temperature sink variable is used everywhere, and background errors are set to 5 K over land (7.5 K over sea-ice), compared to 1 K over sea, to reflect the larger uncertainty in the background values. Secondly, larger surface emissivity errors are taken into account for AMSU-A

Table 1: Usage of surface-sensitive microwave channels considered in the present study. Land surfaces are treated as snow-covered when the surface temperature from the model FG is below 278 K. A sea-ice fraction greater than 0.01 or a sea surface temperature of less than 271.45 K is used to identify areas affected by sea-ice. Some observations over land are subject to orography screening (indicated by "(orog)" in the table), as follows:

Type	Instrument and clear-sky/all-sky	Channel and frequency [GHz]	Snow-free land	Snow-covered land	Sea-ice
T	AMSU-A, clear-sky (on NOAA-15, -16, -18, -19, Metop-A, -B)	5 (53.596±0.115)	yes[1]	yes[1]	N.Hem. only
		6 (54.4)	yes[2]	yes[2]	yes
		7 (54.94)	yes	yes	yes
	ATMS, clear-sky (on S-NPP)	6 (53.596±0.115)	yes[3]	yes[3]	no
		7 (54.4)	yes[4]	yes[4]	no
		8 (54.94)	yes	yes	no
q	ATMS, clear-sky (on S-NPP)	18 (183.31 ±7)	yes[5]	no	no
		19 (183.31 ±4.5)	yes[5]	no	no
		20 (183.31 ±3)	yes[6]	no	no
		21 (183.31 ±1.8)	yes[6]	no	no
		22 (183.31 ±1)	yes[7]	no	no
	MHS, all-sky (on NOAA-18, -19, Metop-A, -B)	3 (183.31 ±1)	yes[7]	yes[7]	yes
		4 (183.31 ±3)	yes[6]	no	yes
		5 190.311	yes[5,8]	no	no
	SSMIS, all-sky (on F-17)	9 (183.31 ±6.6)	yes[5,8]	no	no
		10 (183.31 ±3)	yes[6]	yes[6]	yes
		11 (183.31 ±1)	yes[7]	yes[7]	yes

[1] Except over Antarctica.
[2] Except where orography is higher than 1500 m over Antarctica.
[3] Except where orography is higher than 500 m (1000 m in the tropics).
[4] Except where orography is higher than 1500 m (2000 m in the tropics).
[5] Except where orography is higher than 800 m.
[6] Except where orography is higher than 1000 m.
[7] Except where orography is higher than 1500 m.
[8] Except for latitudes poleward of ±60°.

observations through the physically-based observation error model introduced by Lawrence et al. (2015).

The channels and instruments considered in the present study and their use in the ECMWF system over land and sea-ice are summarised in Table 1 (reflecting data usage in cycle 43r1 for the periods studied here). These are the microwave sounding channels that have some surface-sensitivity; the interpretation of this is somewhat broad - some of the channels (e.g., AMSU-A channel 8) tend to have surface-sensitivity only over elevated surfaces, but over low terrain the surface-sensitivity is negligible. As outlined in Table 1, certain channels are not used over some geographical areas, such as the lowest humidity-sounding channels over snow-covered land. This reflects remaining concerns over our ability to estimate an effective surface emissivity and skin temperature in certain areas. The present study also revealed that there are some inconsistencies in these screening decisions between different instruments, apparent in Table 1: for instance, SSMIS channel 10 at 183.31$\pm$3.0 GHz is used over snow-covered land, whereas the equivalent channel 4 on MHS is presently excluded over these areas; none of the humidity-sounding channels of ATMS are presently used over sea-ice, when equivalent MHS or SSMIS channels are included. These inconsistencies are primarily due to historical reasons, and they have been addressed in cycle 43R3 of the ECMWF system (Weston et al. 2017).

2.2 Experiments

To assess the forecast impact of the surface-sensitive microwave sounding data, assimilation trials were conducted with the ECMWF system for the two four-month periods 2 June – 30 September 2014 and 2 December 2014 – 31 March 2015. Starting from a baseline experiment that does not assimilate the surface-sensitive microwave sounding data listed in Table 1, data is first added over sea-ice, and subsequently data usage is extended to land surfaces, with the humidity-sounding observations added first and then the temperature-sounding data (see Table 1 for the grouping of humidity and temperature sounding data). The following experiments were run:

Base: No surface-sensitive MW sounder data used over land and sea-ice, but otherwise the full operational set of assimilated observations is assimilated.

Base+seaice: As **Base**, but with surface-sensitive MW sounder data added over sea-ice.

Base+seaice+WV land: As **Base+seaice**, but with MW humidity sounder data added over land.

Base+seaice+land: As **Base+seaice+WV land**, but with MW temperature sounder data added over land. The observation usage is hence equivalent to the operational system in 43r1.

All experiments assimilate the observations using ECMWF's 12-hour 4DVAR system, with an incremental analysis resolution at T_L255 ($\approx$80 km), a model resolution at $T_{CO}639$ ($\approx$18 km), and 137 levels in the vertical. 10-day forecasts were conducted from each 00 and 12 Z analysis. All experiments use flow-dependent background errors derived from an Ensemble of Data Assimilations (EDA). For computational reasons, these are taken from the operational system, and the same background error statistics are used for all experiments. The effect of denying observations in our experiments compared to the full operational system is hence not taken into account in the specification of the background errors, but the changes to the background quality are considered sufficiently small for this not to be a large effect.

3 Analysis and forecast impact

3.1 Impact of data over land and sea-ice

We will first discuss the forecast impact of the use of surface-sensitive microwave sounding data over land and sea-ice, respectively, by comparing the experiments **Base+seaice+land**, **Base+seaice** and **Base**. Figure 1 summarises the forecast impact in terms of the change in the headline 500 hPa geopotential root-mean-squared error (RMSE).

There is a clear statistically significant benefit from the assimilation of the data over sea-ice and land (Fig. 1). Adding data over both surfaces leads to a reduction in the forecast error in most geophysical

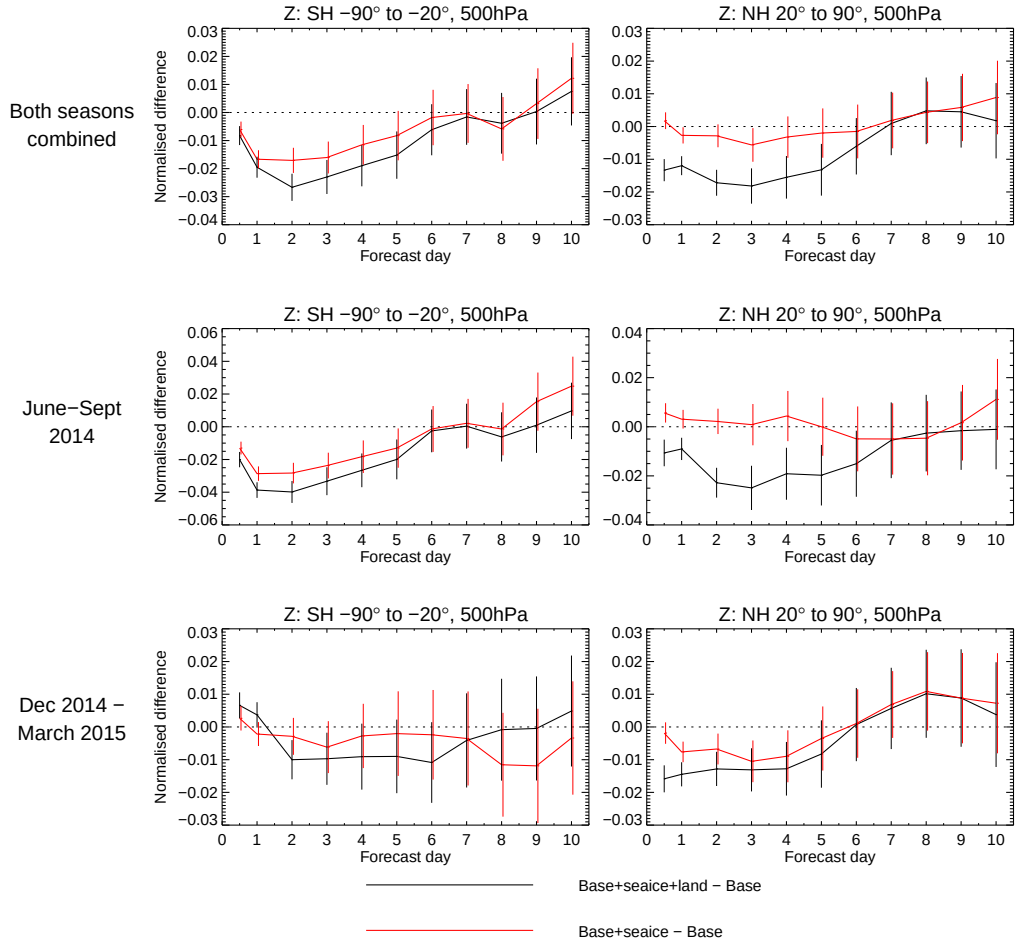

Figure 1: Normalised difference in the RMSE of the forecast of the 500 hPa geopotential as a function of forecast range compared to the **Base** *experiment, for the Southern Hemisphere extra-tropics (left) and the Northern Hemisphere extra-tropics (right). Results are shown for the* **Base+seaice+land** *experiment (black) and the* **Base+seaice** *experiment (red). Each experiment has been verified against its own analysis, and negative values indicate a reduction in the forecast errors from adding the observations. Vertical bars indicate statistical significance at the 95 % level. The top row shows results over the two seasons combined (up to 480 forecasts over 8 months), whereas the middle shows results for the June-September period (up to 241 forecasts over 4 months) and the bottom row results for the December-March period (up to 239 forecasts over 4 months).*

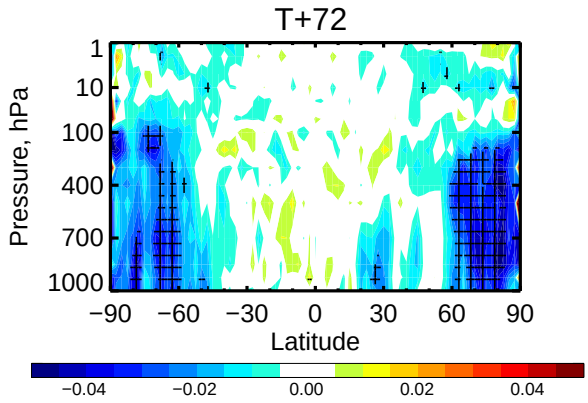

Figure 2: Zonal mean of the normalised difference in the RMS of the forecast error in the 500 hPa geopotential at day 3 between the **Base+seaice+land** *and* **Base** *experiment. Each experiment has been verified against its own analysis, and negative numbers indicate a reduction in the forecast errors from adding the observations. Hatching indicate statistical significance at the 95 % level. Results for the two seasons considered here have been combined.*

variables of typically 1-3 % up to day 5 compared to the **Base** experiment, with a similar impact in terms of the standard deviation of the forecast error. Most of this impact is primarily found at higher latitudes (Fig. 2), ie areas covered by sea-ice, but also remote land areas such as Siberia and Northern Canada which are more poorly covered by conventional observations. The forecast impact over the tropical regions appears to be relatively limited. This is consistent with a relatively smaller impact of microwave sounding observations in tropical regions in general (e.g., McNally et al. 2014), together with a smaller extent of land-covered surfaces and hence smaller changes in the data usage in these experiments.

As expected, there is a very clear seasonal dependence of the forecast impact, reflecting, for instance, the much larger sea-ice extent over the Southern Hemisphere during the June-September period (cf the middle and lower row in Fig. 1). Adding the data over land also shows seasonal dependence over the Northern Hemisphere (compare the black and the red lines in the right column of Fig. 1), with considerably larger impact over the summer period. This is likely to be linked to the larger extent of the snow cover during winter and the relatively reduced data usage over these surfaces (see section 5.2). We will further discuss the impact of specific geographical regions when we examine results from adjoint-based forecast impact diagnostics.

The beneficial forecast impact from the microwave sounder data over land in the short-range is also demonstrated through improved background fits to conventional observations (cf the black and the red line in Fig. 3a-c). The benefit of the data over sea-ice is less clear in these hemispheric statistics, but standard deviations of background departures for radiosondes over the polar regions only also confirm a beneficial impact (Fig. 4, left). In addition, the background fit to lower tropospheric hyperspectral infrared satellite observations is significantly improved through the assimilation of the data over sea-ice (e.g., see red line Fig. 3d), consistent with the impact previously noted in analysis-based forecast scores. The IASI observations also confirm significant benefits in terms of humidity (see channel numbers larger than 1639), primarily from the assimilation of the microwave sounding data over land. This is consistent with the significant improvements seen for humidity from radiosondes (Fig. 3b). The finding is, however, remarkable, as IASI observations are not assimilated over land, so the noted effect must be due to accumulated benefits advected downstream from the affected land areas.

The assimilation of the MW sounding data over sea-ice introduces a significant change to the mean temperature and humidity analyses at lower levels over the regions covered by sea-ice (e.g., Fig. 5), as

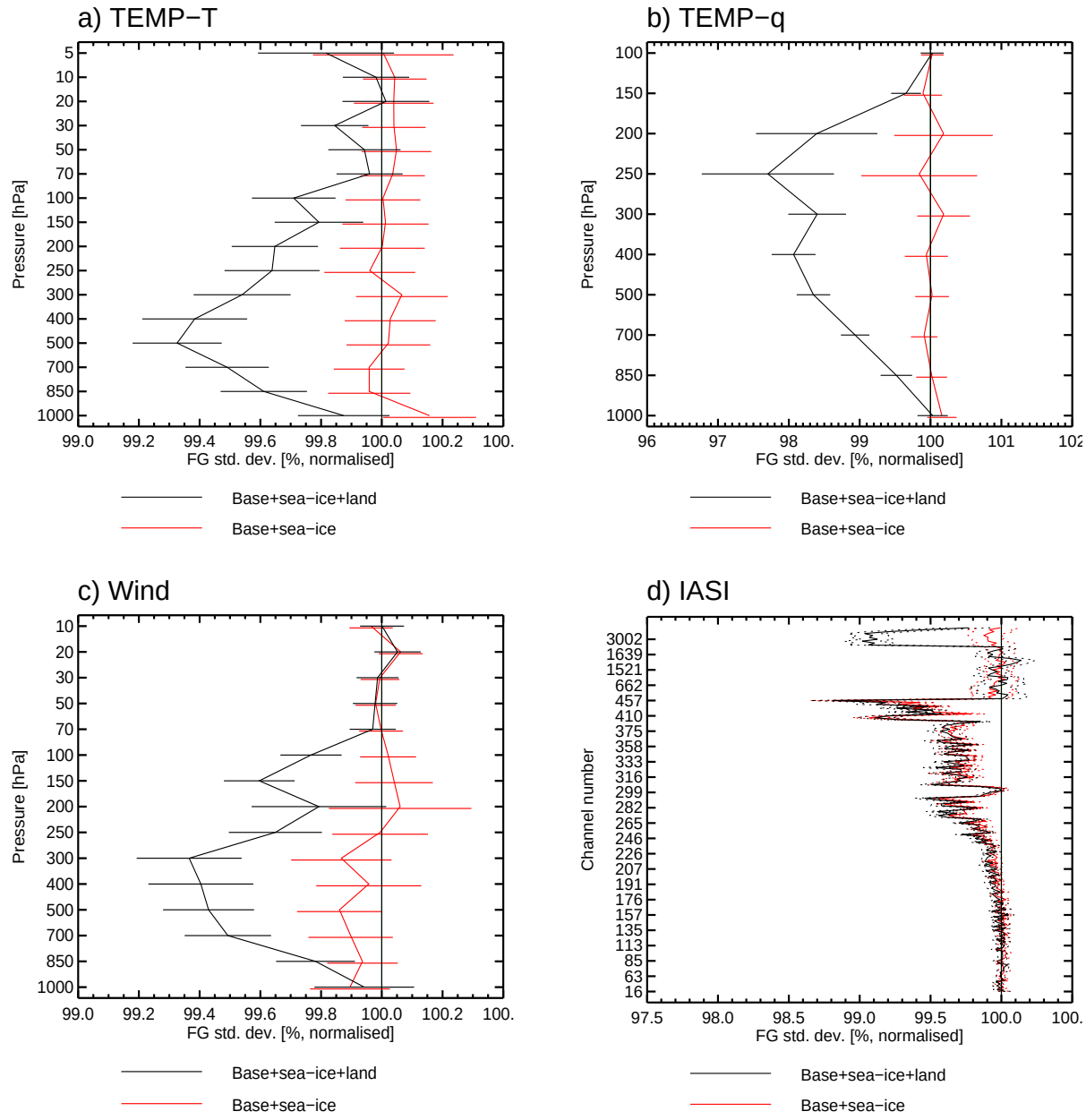

Figure 3: a) Standard deviation of background departures for assimilated temperature observations from radiosondes for the **Base+seaice+land** *experiment (black) and the* **Base+seaice** *experiment (red), both normalised by values for the* **Base** *experiment. Horizontal bars indicate statistical significance at the 95 % level. Results for the two seasons considered here have been combined, covering a total of 8 months. b) As a), but for humidity observations from radiosondes. c) Ad a), but for conventional wind observations (from sondes, aircraft, and profilers). d) Ad a), but for observations from the IASI instruments on Metop-A and Metop-B. Here, dotted lines indicate 95 % confidence intervals.*

previously reported by Di Tomaso et al. (2013) for the introduction of MHS data over sea-ice . For the Southern Hemisphere winter season, the mean temperature at 850 hPa is typically 0.1-0.8 K warmer around Antarctica with the MW sounding data over sea-ice included (Fig. 5b). Radio-sondes provide some support for this change, indicating the reduction of a considerable cold bias at 850 hPa, at least

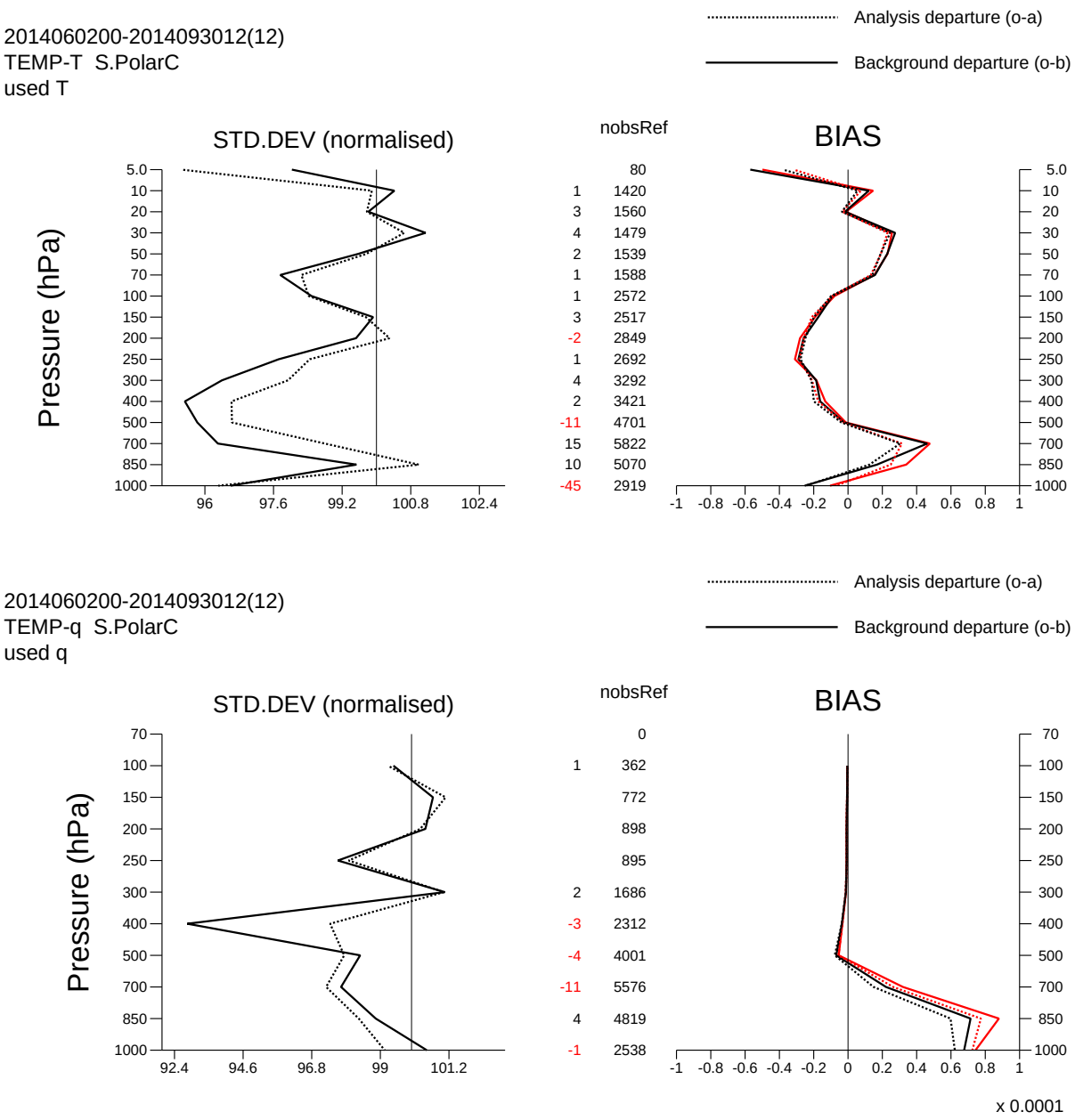

Figure 4: Top row: Background (solid) and analysis (dotted) departure statistics for used radiosonde temperature observations in the South Polar region for the June-September period. Standard deviations from the **Base+seaice** *experiments are shown on the left, normalised by values from the* **Base** *experiment [%]. Biases [K] are displayed on the right, with values from the* **Base** *experiment in red and from the* **Base+seaice** *experiment in black. Bottom row: As above, but for radiosonde humidity observations, with biases in kg/kg.*

over the coastal areas where most radiosondes reside (Fig. 4, top right). Note, however, that at 1000 hPa this turns into a warm bias of the analysis against the radiosondes. It appears that the data is partly correcting a previously present bias, but there are also indications for an over-correction, likely to be linked to biases in the surface emissivity retrieval over snow and sea-ice, further discussed in section 5.2.

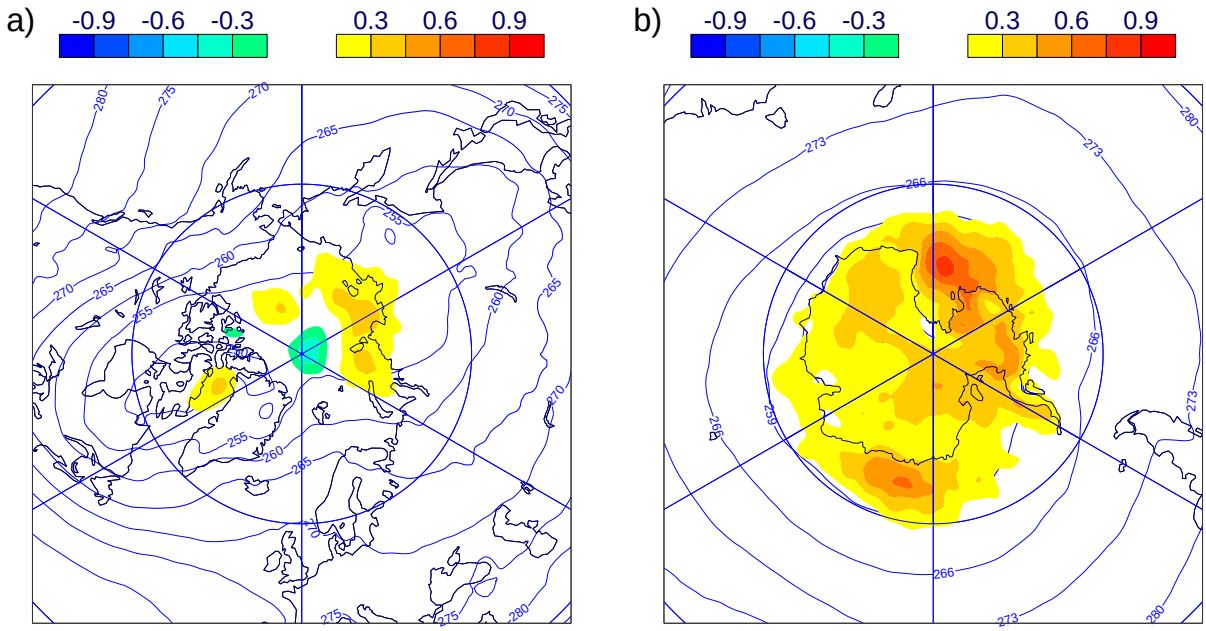

Figure 5: Differences in the mean temperature analyses at 850 hPa between the **Base+seaice** *and the* **Base** *experiment [K] for the respective winter seasons, ie a) for the December-March period over the Arctic regions, and b) for the June-September period over Antarctica.*

3.2 Impact of temperature and humidity sounding data over land

Next we will investigate the respective impact of adding the humidity and the temperature sounding microwave data over land. Here, we compare the experiments **Base+seaice+land** and **Base+seaice+WV land** to **Base+seaice**. Note that we do not compare here the separate addition of temperature and humidity sounding data over land, respectively, but instead the effect of adding the two types of data sequentially, and we add the temperature-sounding data in the presence of the humidity-sounding data. It could be argued that this favours the humidity-sounding data, as it is added first, making it easier to

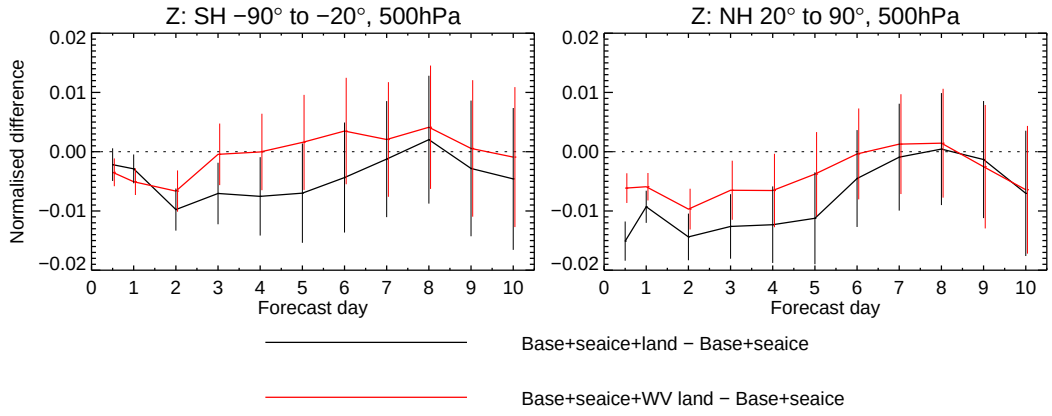

Figure 6: Forecast scores for both seasons combined, as in the top row of Fig. 1, but for the comparison of the **Base+seaice+land** *(black) and the* **Base+seaice+WV land** *experiment (red) to the* **Base+seaice** *experiment.*

lead to improvements. But it could also be argued that it favours the temperature-sounding data, as any potential benefits from a synergistic use of humidity and temperature sounding data (e.g., in terms of better distinction of temperature and humidity/cloud signals) will appear as benefits from the addition of the temperature-sounding data.

Both, the temperature and the humidity sounding data show a statistically significant reduction in the forecast errors for the geopotential or temperature over the troposphere (e.g., Fig. 6). This is particularly the case for the Northern Hemisphere where most of the data is added and forecast benefits are significant up to day 4-5. For the Northern Hemisphere, the benefit of adding the temperature-sounding data in addition to the humidity-sounding data is roughly similar in magnitude to the benefit of initially adding the humidity-sounding data. Over the Southern Hemisphere, the impact is less statistically significant, owing largely to the smaller amount of land and hence the smaller number of observations added in these experiments.

As noted earlier, there is considerable seasonal dependence of the forecast impact. The reduction in the forecast error for adding the temperature and humidity sounding data over the Northern Hemisphere reaches around 3 % for the summer period, whereas it stays mostly below 1 % for the winter season (Fig. 7). Over the winter season, the benefits are almost entirely achieved by the humidity sounding data, whereas the further impact of adding the temperature sounding data is mostly neutral for this season. This is particularly note-worthy as the assimilation of the humidity-sounding data over snow-covered surfaces is limited to channel 3 of MHS and channels 10 and 11 of SSMIS in these experiments and other channels are rejected outright. In contrast, all channels considered here for the temperature-sounding data are considered for assimilation over snow, even though many fail the quality control check on the departures of the 50.3 GHz window channel, such that the proportion of actually assimilated data is lower than over snow-free land surfaces. We will get back to this aspect in sections 4 and 5.2.

The short-range forecast impact is further highlighted by considering the standard deviation of background departures for a selection of observations in Fig. 8. Consistent with the medium-range scores,

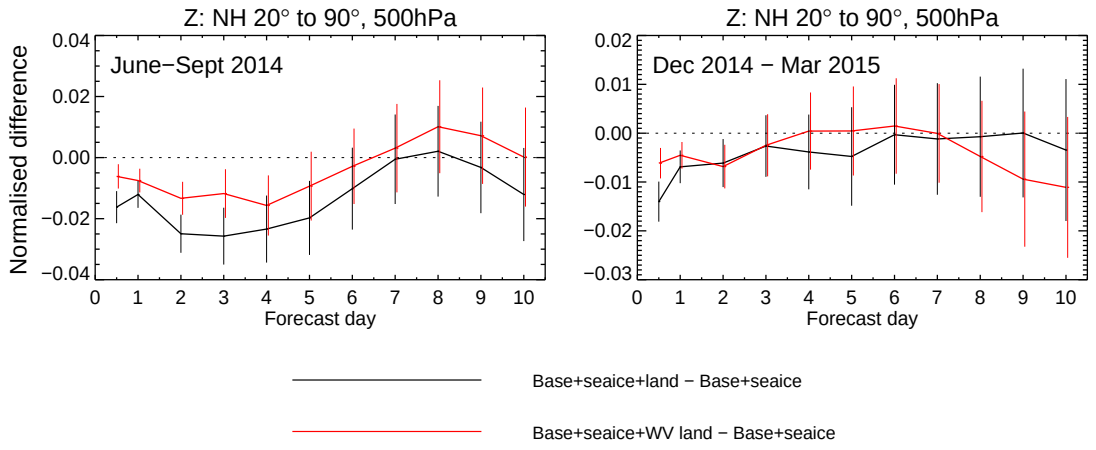

Figure 7: Normalised difference in the RMSE of the forecast of the 500 hPa geopotential as a function of forecast range compared to the **Base+seaice** *experiment, for the Northern Hemisphere extra-tropics. Results are shown for the* **Base+seaice+land** *experiment (black) and the* **Base+seaice+WV land** *experiment (red), and the left panel shows results for the June-September periods, whereas the right panel shows results for the December-March period, each covering four months. Each experiment has been verified against its own analysis, and negative numbers indicate a reduction in the forecast errors from adding the observations. Vertical bars indicate statistical significance at the 95 % level.*

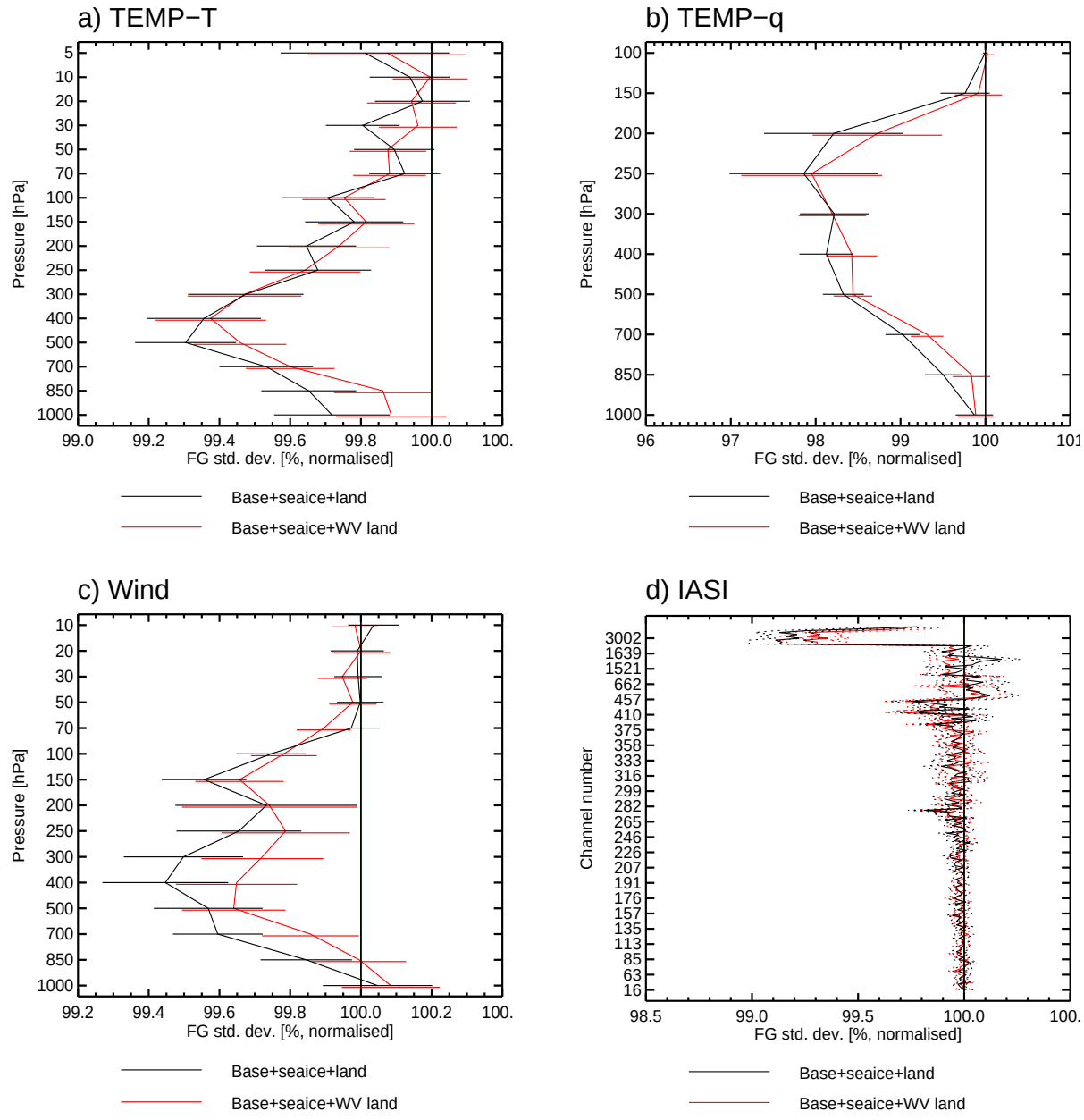

Figure 8: As Fig. 3, but for the comparison of the **Base+seaice+land** *(black) and the* **Base+seaice+WV land** *experiment (red) to the* **Base+seaice** *experiment.*

these indicate statistically significant reductions in short-range forecast errors from adding the humidity-sounding data over land, with further statistically significant benefits for temperature and wind observed by radiosondes from adding the temperature-sounding data over land. Interestingly, for temperature observations from radiosondes, the signal from adding the humidity-sounding data appears to be stronger than the additional benefit from adding the temperature-sounding data. This is likely due to adjustments in response to the dynamical information implicitly provided by the humidity-sounding observations.

4 Forecast Sensitivity to the Observation Impact

We will now attempt a more detailed assessment of the impact of surface-sensitive microwave data considered here in terms of the geographical distribution of their impact. This will be done using the adjoint-based Forecast Sensitivity to the Observation Impact diagnostic (FSOI; e.g., Langland and Baker 2004, Cardinali 2009). In the ECMWF system, this measure provides an estimate of the impact of an observation in terms of reducing the overall 24 h forecast error, weighted by a global dry total energy norm. For technical and computational reasons, the statistics presented here are taken from the operational ECMWF system, rather than the previously discussed experiments. In order to use the version of the ECMWF system consistent with that used in the previous section, we present results not for the same period, but rather the corresponding period in 2016. This ensures that the data selection for the instruments considered, and in particular the coverage over land and sea-ice is consistent. Note, however, that the June-September 2016 period includes the assimilation of 183 GHz channels from MWHS-2 which was not used in the observing experiments presented in the previous section, and hence will also not be included in the FSOI statistics here. As cycle 41r2 only became operational on 8 March 2016, we only show statistics for the last 23 days of March 2016 for the second season.

Figure 9 shows maps of the distribution of the combined FSOI of the channels considered here. An equal-area display with accumulations over equal-area boxes is chosen to more appropriately compare different regions of the globe. Globally, the temperature-sounding channels shown in these maps contribute 10.9 % to the overall FSOI for all observations, with the humidity-sounding channels contributing 12.6 %. The detailed interpretation of these maps is not always straightforward, as the values will be influenced by a range of factors unrelated to the use of surface-sensitive observations over land, including the temporal positioning of the data within the assimilation window. Also, FSOI uses an analysis to estimate forecast errors, and while this is arguably the best estimate of the true atmosphere, this practice is likely to be plagued by general problems with analysis-based verification in the short-range, related to correlations between analysis and forecast errors. This is particularly problematic in the tropics. In addition, the influence of model bias on FSOI estimates is somewhat unclear and has been found to give mis-leading results (e.g., Cardinali and Prates 2009).

Despite these caveats, FSOI indicates rather strong impact over remote land areas at higher latitudes, such as over North-Eastern Canada and Siberia, and over the Southern Hemisphere sea-ice. This is overall consistent with expectations and with the results from the observing system experiments discussed earlier. Over the more remote higher latitude regions, the impact is helped by the relatively frequent sampling provided by the polar satellites, leading to elevated observation counts. The sea-ice regions are associated with some of the largest FSOI contributions, despite a more restrictive data usage in this area resulting from the difficulties of estimating surface emissivity. The relatively large contribution over sea-ice, albeit over quite a small area, is consistent with the considerable impact from the OSEs when data over this region is denied. For the June-September period, the FSOI contributions for the temperature and humidity sounding observations shows overall a relatively similar pattern over these more remote higher latitude areas.

Comparisons between Figures 9 and 10 reveal, among other things, the impact of the reduced data usage in snow-covered areas over the Northern Hemisphere. This is particularly noticeable for the humidity-sounding channels, where the lowest sounding channels are rejected outright in regions with surface temperatures below 278 K and hence potential snow cover. The temperature-sounding channels fare a little better in terms of FSOI contributions in these snow-covered areas. This is even though the impact is less apparent in the OSEs discussed earlier.

For the temperature-sounding data, some of the largest FSOI contributions are found over the Sahel

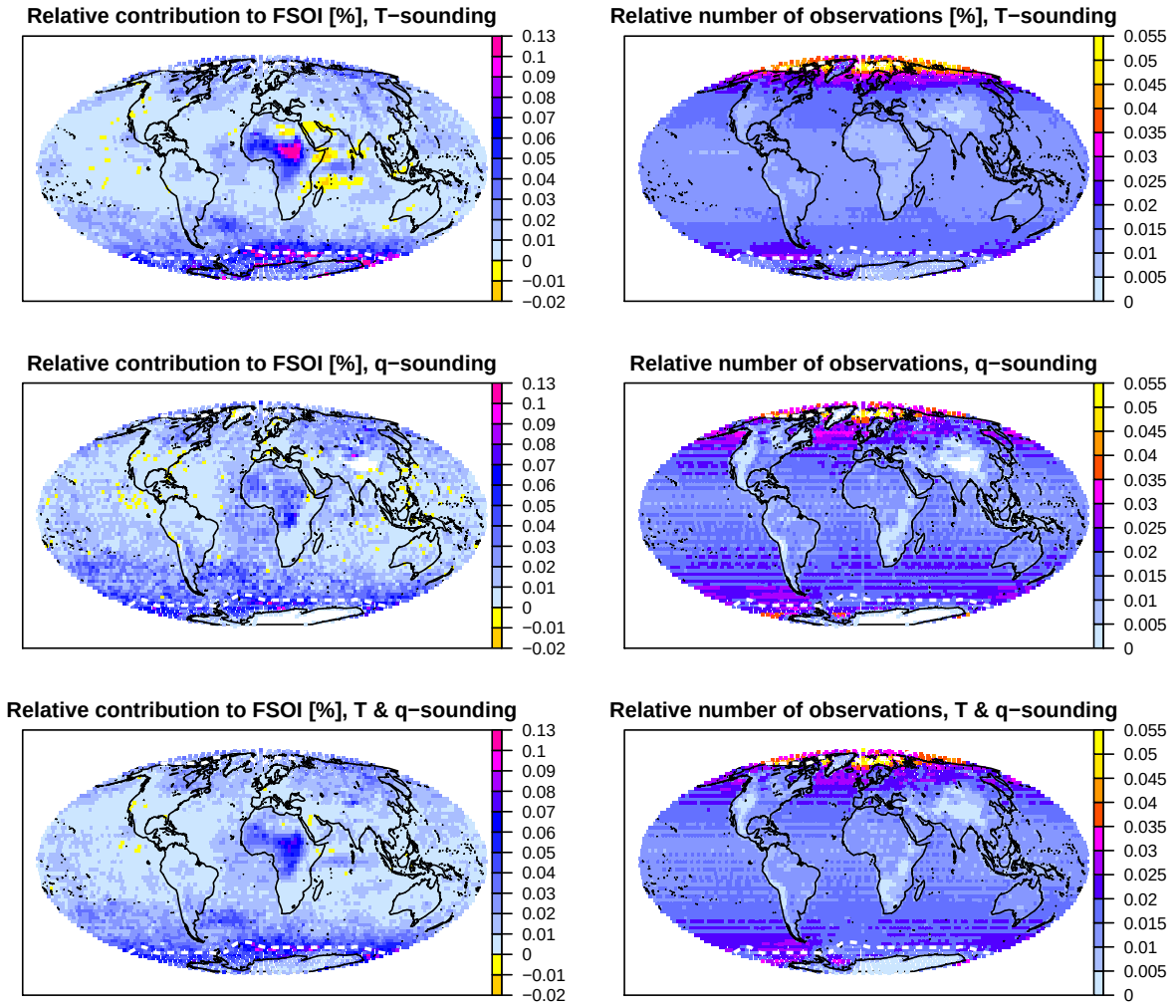

Figure 9: Maps of contributions to the total FSOI (left column) and the number of observations (right column) for the operational ECMWF system over the period 2 June - 30 September 2016. The top row shows statistics for the surface sensitive microwave temperature-sounding channels of AMSU-A and ATMS, the middle row the microwave humidity-sounding channels of MHS, ATMS, and SSMIS, and the bottom row the combined statistics. Normalisation is always such that the sum of all contributions for the sub-set of data shown gives 100 %, and positive values indicate a reduction in forecast error. Binning is in equal-area boxes, with the size corresponding to 2.5×2.5° at the equator. Dashed white lines indicate the average sea-ice border for the period shown.

region for the June-September period and over the Congo Basin in March. This is in contrast to the more neutral medium-range forecast impact of the data over land in the tropical region found earlier in the OSE. The feature is most prominent in AMSU-A channel 6 (ATMS channel 7), sensitive to temperature around 200-700 hPa. This most likely reflects an interaction with the diurnal cycle of the convection scheme while the Intertropical Convergence Zone is positioned over the regions in question. The feature appears to be largest between local solar times (LTs) of 21 - 9 hours, as can be seen in Fig. 11(top) which shows the FSOI per observation over a box covering the feature in question over the wider Eastern Sahel region (see Fig. 12 for the positioning of the box). The FSOI contribution is shown as a function of the

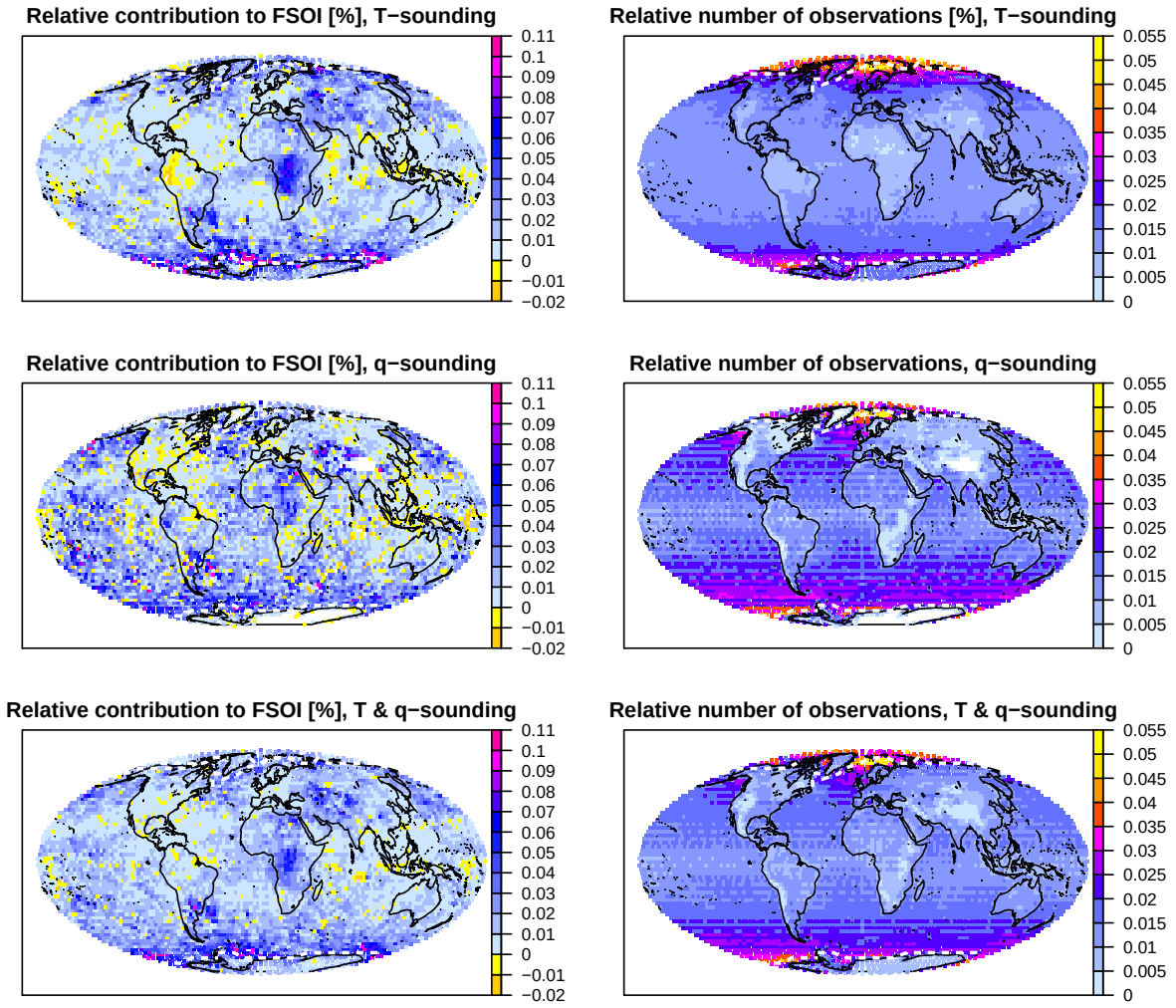

Figure 10: As Fig. 9, but for the period 8 - 31 March 2016.

temporal positioning of the satellite over-passes in the assimilation window (x-axis), since observations towards the end of the 12-hour assimilation window tend to have larger impact (e.g., Cardinali 2014). Colours indicate the LT. For similar positions within the assimilation window, observations with an LT between 21 and 9 hours show much larger FSOI contributions, especially for channel 6, whereas FSOI instead even suggests some detrimental impact between 12 and 15 LT.

The feature of enhanced FSOI is also associated with considerable biases in the assimilated observations. Between 21 and 9 hours LT mean channel 5 or 6 departures in the region suggest that the background is, on average, too cold compared to the observations, whereas mean departures suggest that the background is too warm around mid-day (bottom row of Fig. 11). The warm bias in the departures at night-time is unlikely to be residual cloud contamination, but may instead be the result of a lack of night-time convective rain in the ECMWF model, associated with insufficient latent heating (e.g., Bechtold et al 2014, Lopez 2014)[1]. The region is also an area where the introduction of the data considered here leads

[1]Note that this is distinct from the finding of Chambon and Geer (2017) that the diurnal cycle of all-sky humidity-sounding

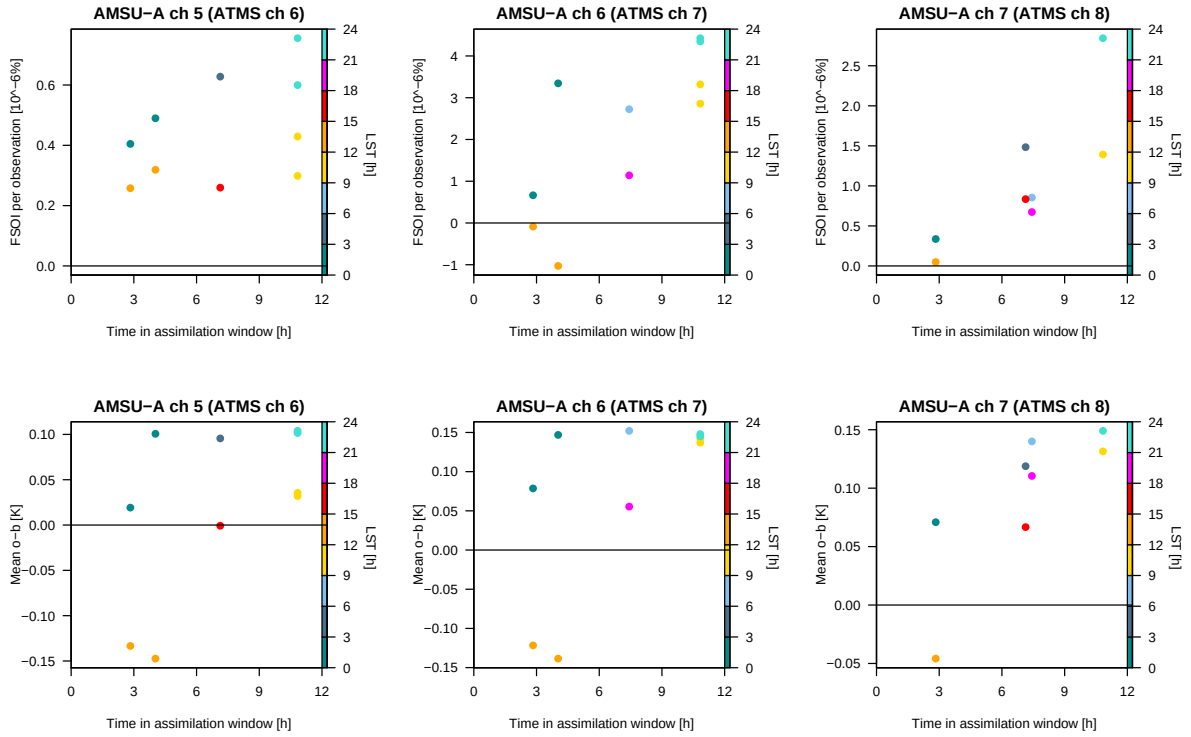

Figure 11: Top row: Contribution to the FSOI per observations over the wider Eastern Sahel region (0 to 18 N; 15 to 35 E) from the ECMWF operational system during the period 2 June to 30 September 2016 for the three microwave temperature-sounding channels considered here. The values are shown in terms of the positioning of the satellite over-passes within the assimilation window (x-axis), and colour coded by the LT (h). Bottom row: As top row, but for the mean departures after bias correction for the assimilated observations.

to some of the largest changes in the size of the increments in the OSEs (not shown). At this point, it is not clear whether the larger FSOI contributions are a true signal of more influential observations, or instead an artifact, resulting from issues with the verifying analysis and diurnal model biases. A similar, but weaker signal can be found in the humidity-sounding data for the June-September period (Figure 9 and 10, middle).

Areas with lower FSOI contribution from the surface-sensitive MW radiances over land are primarily found over areas relatively well-observed by conventional observations (e.g., Europe, USA, Eastern China), regions of more restricted data usage such as higher terrain or snow, as well as some desert regions (Figure 9 and 10). The desert regions show particularly low impact from the microwave temperature sounding channels (e.g., over the Sahara, Arabian peninsula, Australia), whereas the humidity sounding channel fare better in some of these regions (especially the Sahara). The smaller FSOI contribution may be related to problems in the estimation of the surface emissivity due to diurnal biases in the skin temperature estimates used for emissivity estimation. This aspect will be discussed further in section 5.1.

departures over land suggests that convective clouds are well represented in the ECMWF system at night-time.

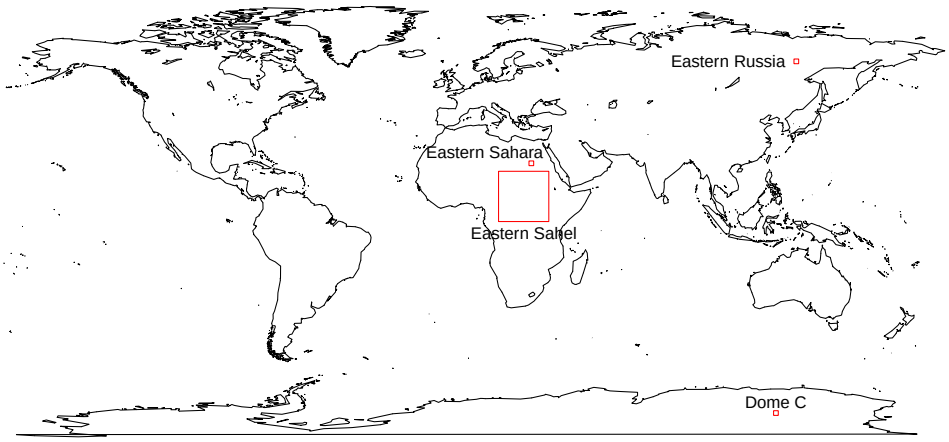

Figure 12: Locations of regions of interest considered in this study.

5 Issues

The previous sections have highlighted the value of the assimilation of surface-sensitive microwave data over land and sea-ice in the present operational ECMWF system. It is clear that the present approaches are capable of extracting useful information from the assimilated observations, and the data contributes positively to forecast skill.

Nevertheless, it is worth critically assessing where the present approaches exhibit short-comings and where there are areas of potential improvements, also with a view of increasing data usage. In the following, we will summarise such areas and investigate some in more detail. One aim is to identify areas for future developments, in particular, where there are over-arching issues that require new assimilation approaches.

Figure 13 shows departure statistics for NOAA-19 AMSU-A channel 5, the most surface-sensitive temperature-sounding channel considered in the ECMWF assimilation system. For most regions, these statistics look as expected: standard deviations of background departures are a little larger over land than over sea, indicative of larger errors associated with emissivity and skin-temperature error over land, and this is addressed through the setting of larger observation error and larger background error for the skin temperature (Lawrence et al. 2015). Mostly, biases are also at similar levels over land as over ocean and for many regions the number of observations that pass quality control is at a similar level as over ocean. However, there are specific areas for which this is not the case, and these are the areas typically seen as "difficult" for the assimilation of surface-sensitive radiances:

Desert: Reduced data usage is apparent over some desert regions (e.g., Sahara, Arabia) for both periods. Some of these areas are also associated with larger standard deviations of background departures. There is no specific quality control implemented for desert regions, so the rejections are the result of more general quality control steps designed to eliminate observations which are not sufficiently modelled by the background. Note, however, that some desert regions do not show clear signs of

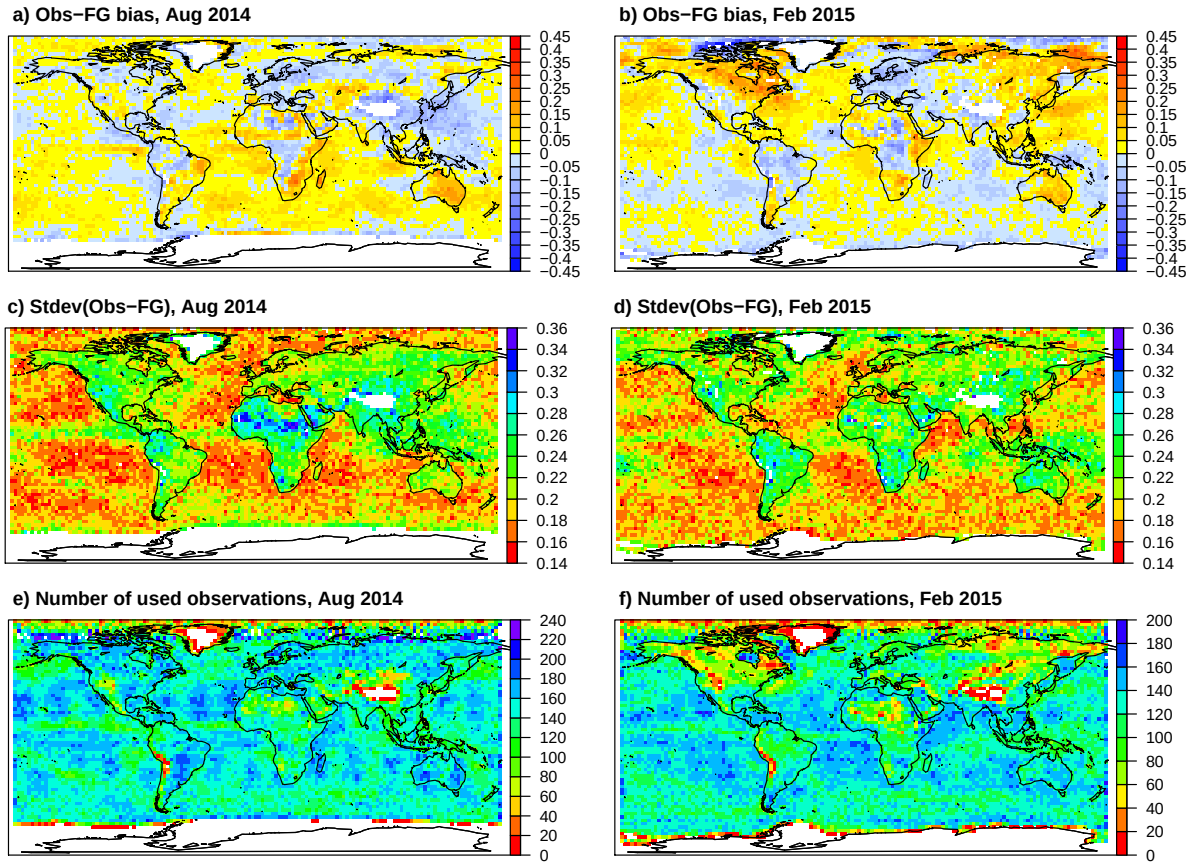

Figure 13: a) Bias between observations and background for assimilated AMSU-A channel 5 observations from NOAA-19 after bias correction for August 2014 for the **Base+seaice+land** *experiment introduced in section 2. b) As a), but for February 2015. c) As a), but for the standard deviation of background departures. d) As c), but for February 2015. e) Number of used observations for AMSU-A channel 5 from NOAA-19 for August 2014 for the* **Base+seaice+land**. *f) As e), but for February 2015.*

higher rejections, most notably Australia.

Snow: For the February period, regions over the Northern Hemisphere with heavy snow cover (e.g., Canada, Siberia) show larger positive biases and also much reduced data usage compared to the August period. Again, there is no specific exclusion of data over snow-covered areas, but it appears that we do not model the observations as well in these situations as elsewhere, prompting general quality control steps to exclude these observations. It is worth noting that the projection used in Fig. 13 emphasises the effect, both in terms of the low number of observations and the affected areas. These high-latitude areas are also the regions that benefit most from the better sampling of polar-orbiting satellites, and on a per-area basis the number of used observations is not necessarily worse than, say, in tropical regions over sea (compare Fig. 10 for an equal-area projection of this). Nevertheless, the larger number of rejections indicates some issues with the current data usage.

Sea-ice: The February period also reveals larger biases (positive as well as negative) and elevated standard deviations over Northern Hemisphere sea-ice regions. For the Southern Hemisphere, sea-ice regions are rejected explicitly.

High orography: For regions with high orography, the channel shown will have stronger surface-sensitivity

and hence the contribution from the uncertainties in the surface modelling become too large. This aspect is estimated through the situation-dependent observation error (Lawrence et al. 2015), and the rejections are due to the estimate of this uncertainty contribution becoming too large. The channel will also contain less information on the atmosphere here, providing less incentive to optimise the assimilation.

To further complement the above, Fig. 14a shows the temporal evolution of the surface emissivity estimate used in the assimilation over a 9-month period for a region in Eastern Russia (just East of Yakutsk, see Fig. 12). The area shows fairly homogeneous vegetation, covered primarily by boreal forest. For

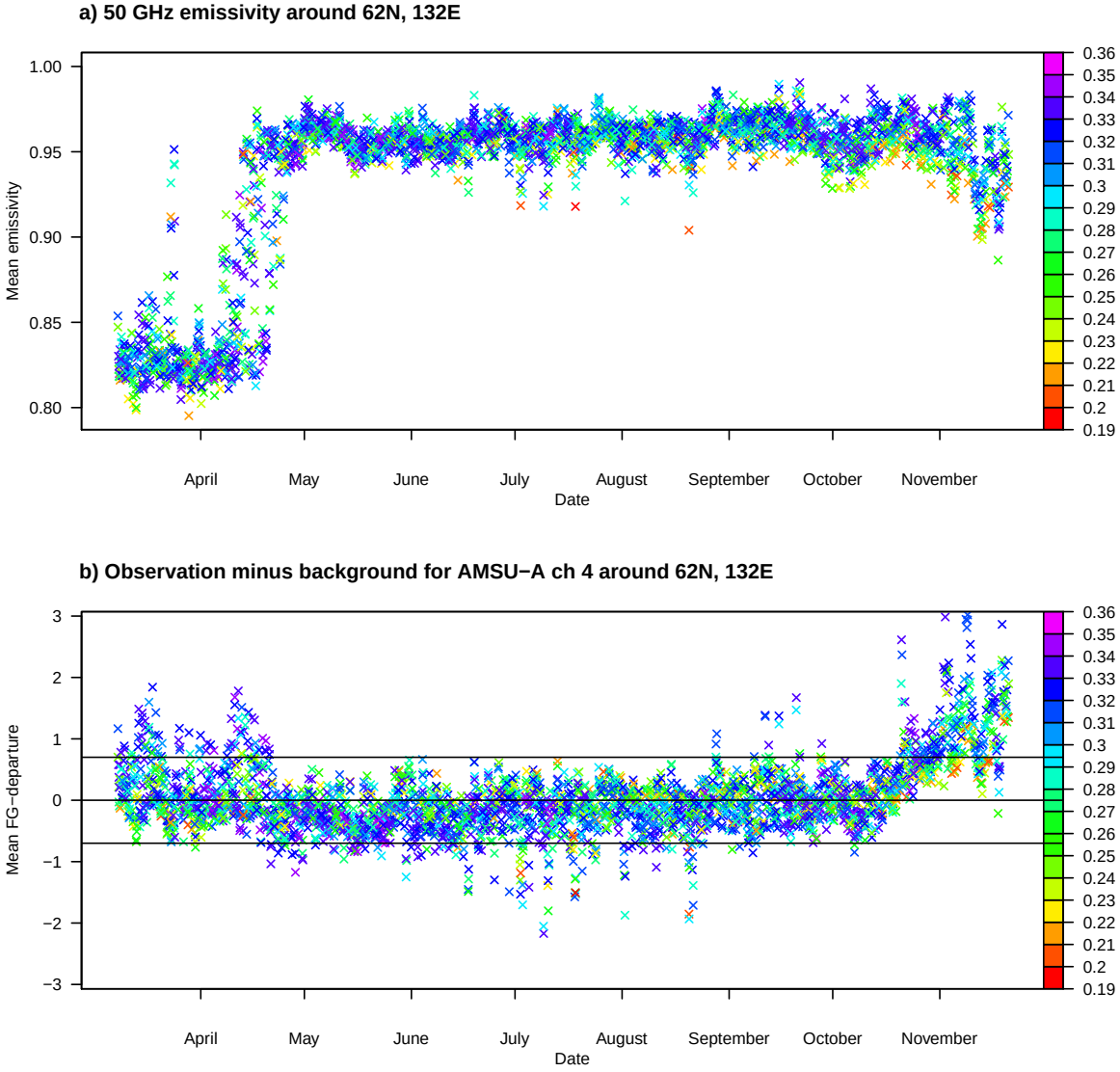

Figure 14: a) Estimated emissivity for the 50 GHz sounding channels for a 2×2° box around 62N, 132E in Eastern Russia, east of Yakutsk. The values are 12-hourly means over all available AMSU-A and ATMS data, separated by satellites, and they are taken from ECMWF's operational High-resolution system. Colour coding indicates the mean surface-to-space transmittance. b) Mean observation minus background departure in AMSU-A channel 4 (or ATMS channel 5) for the same observations and sampling as in a).

large parts of the year, the dynamically estimated emissivity shows only little variation, staying within a narrow band of ± 0.01 in terms of day-to-day variation, and with some small seasonal differences, possibly linked to changes in vegetation. Some of the day-to-day scatter in the retrieved emissivities during this period may be linked to real effects, such as polarisation differences in the observations resulting from different viewing geometries or sudden changes in the surface characteristics. But some variability will also be erroneous, resulting from aliasing of background errors or cloud contamination into the emissivity estimate. In any case, the slow evolution of the emissivities and the relatively confined scatter shown for the period May to mid-October in Fig. 14 is a typical example for many non-desert, lower altitude regions with no snow cover. The behaviour underlines that an appropriate atlas, possibly slowly evolving in time, should be at least as adequate for the specification of surface emissivity as the dynamic emissivities in these cases.

However, Fig. 14a also shows some deviations from the slow evolution: most notably, there are strong variations in surface emissivity at times during the spring months or late November, associated with changes due to snow during these periods. Here, day-to-day variability can become large, indicating either actual temporal changes in the snow morphology or cover, or larger uncertainty in the estimated emissivity. During this time, channel 4 departures show a tendency for larger positive departures. It is already clear from this that snow provides a larger challenge for the surface emissivity specification.

Fig. 14a also highlights another issue: even during the summer months there are occasions during which the emissivity estimates drop suddenly outside the previously confined band. The times tend to be associated with sizeable channel 4 departures (below -1 K). The large departures in channel 4 suggest that the background calculations for channel 4 are not consistent with observations. Further investigation shows that these are mostly instances of strong and persistent cloud/rain contamination. Neglecting cloud/rain contributions in the emissivity retrieval leads to the lower emissivity estimates for these occasions. This aspect will be further discussed in section 5.3.

In summary, this overview has highlighted potential short-comings in the assimilation of surface-sensitive microwave data over desert, snow, and related to cloud detection, at least in the temperature-sounding channels. In the following, we will investigate these aspects in some more detail in turn.

5.1 Desert

The above overview has highlighted that desert regions appear particularly challenging to use for microwave temperature sounding observations at 50 GHz, as evident through fewer observations passing the quality control checks in these regions. This has been analysed in further detail, through departure statistics over a number of small areas in desert regions. As an example, we will discuss here the performance over a $2\times2^{\circ}$ region in the Eastern Sahara (centred at 22N, 28E, see Fig. 12). Departure statistics for this area are very typical of a range of other desert sites, such as elsewhere in the Sahara or in the Arabian or Kalahari deserts.

Making use of the different satellites with varying over-pass times, Fig. 15 shows the mean diurnal cycle in channels 4-6 of AMSU-A (and 5-7 of ATMS) over the selected region. Very large positive departures (too low FG) are apparent during night-time and less severe negative departures during day-time. The Figure is based on all data before quality control, and it is clear that many night-time observations will be rejected through the strict departure check for channel 4 (requiring the absolute value of channel 4 departures to be less than 0.7 K). This is the main mechanism why fewer observations are used over desert regions in our experiments. The biases in the sample of observations that are allowed to affect the analysis are therefore much smaller, and the quality control successfully protects the analysis from the

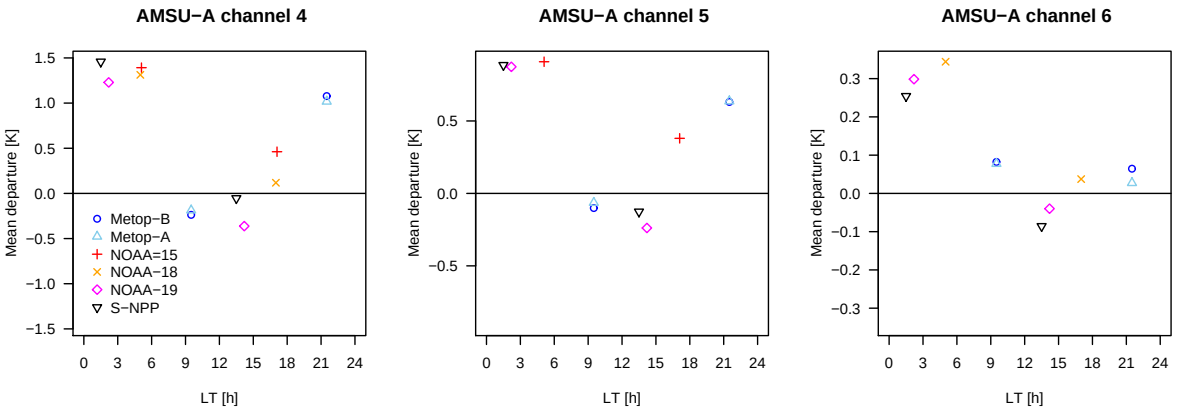

Figure 15: Mean FG departures after bias correction in AMSU-A channel 4 (left), channel 5 (middle) and channel 6 (right) as a function of the local solar time associated with the satellite over-pass for all observations with a zenith angle of less than 20 ° over a 2°×2° area centred around 22N 28E in the Eastern Sahara desert. The period is June to August 2014 and the statistics are taken from the **Base+seaice+land** *experiment introduced in section 2. Also included are departures for equivalent ATMS channels flown on S-NPP (channels 5 to 7, respectively).*

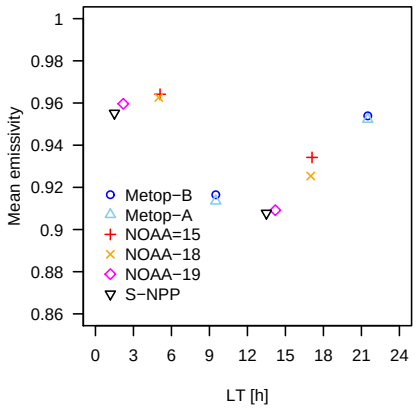

Figure 16: Mean surface emissivities retrieved from channel 3 observations of AMSU-A (channel 4 of ATMS) as a function of the local solar time associated with the satellite over-pass over a region in the Eastern Sahara. The data selection and area are the same as in Fig. 15.

worst biases. However, the rejections are not due to cloud-affected observations, as cloud contamination is negligible over this site. As similarly strong day/night differences are not found elsewhere, the origin of these diurnal biases is most likely local biases in the FG or the radiative transfer calculations.

The diurnal biases in the FG departures are associated with significant diurnal variation in the retrieved surface emissivity, as displayed in Fig. 16. Variations of around 0.05 are apparent, larger than expected over desert regions with stable surface conditions (e.g., Grody and Weng 2008). Figure 17 shows that similar relatively large day/night differences in the retrieved surface emissivities occur over many other desert regions. Aside from over the Sahara, similar characteristics are found especially for the Arabian, Kalahari or Taklamakan (Western China) deserts, with the magnitude somewhat seasonally dependent (not shown).

Further investigations show that the diurnal characteristics displayed are consistent with very sizeable

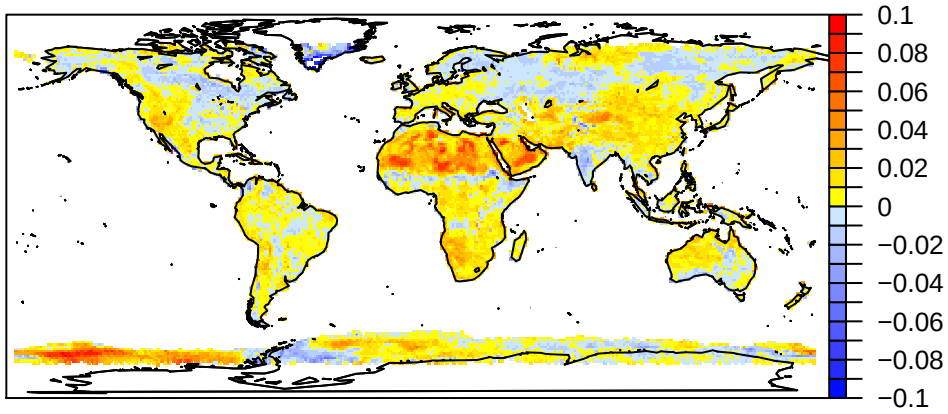

Figure 17: Difference in the mean retrieved surface emissivity at 50.3 GHz between night (1:30) and day (13:30) obtained for ATMS over the period June-August 2014. Data is binned in 1x1° boxes and all emissivity retrievals from observations with a zenith angle less than 20° have been considered, with no attempt to screen for clouds.

diurnal biases in the temperature used to determine the surface radiation. Biases in this temperature will affect the retrieved surface emissivity, and any diurnal biases will lead to an erroneous estimate of diurnal variation of emissivity. This will then affect the subsequent radiative transfer calculations for the sounding channels. The biased emissivity estimate will partially mask the surface temperature biases for the sounding channels, but some biases will nevertheless remain due to the surface reflection term in the radiative transfer equation and different surface-sensitivity in the two channels. A similar diurnal behaviour has been found for emissivities retrieved from SSMIS imaging channels over desert regions by Baordo and Geer (2016). The aspects are explored more quantitatively in the following using a simulation approach.

The simulation of the effect is based on atmospheric profiles and skin temperature information extracted from the ECMWF FG at S-NPP ATMS locations over a similar desert region during two days in July 2015. We use S-NPP ATMS, as it exhibits some of the clearest day/night bias differences (due to the 1:30/13:30 LT overpass times), and offers an additional surface-sensitive channel (channel 4 at 51.76 GHz) not available on AMSU-A. The atmospheric profiles and skin temperature values are treated as "truth", combined with surface emissivity estimates retrieved from ATMS observations, and together these are used to first simulate "true" (clear-sky) observations, as illustrated in Fig. 18 (see "True T_B"). We then perform an emissivity retrieval with these "true" observations, using radiative transfer terms determined by the "true" atmospheric profiles, but with a bias added to the "true" surface temperature. This results in a retrieved perturbed emissivity. Together with the biased surface temperature this is subsequently used again in radiative transfer calculations for the sounding channels, to lead to perturbed brightness temperatures (see "Perturbed T_B on right-hand-side of Fig. 18). These can then be compared to the "true" observations to obtain the effect of the bias added earlier to the skin temperature. All radiative transfer calculations are restricted to clear-sky. The results are summarised in Fig. 19 through blue triangles, plotted as a function of surface-to-space transmittance, a useful coordinate to display the results from several channels. Also shown are mean observed departures from S-NPP ATMS, with night-time values indicated through stars and day-time values through dots.

Figure 19 illustrates that an 8 K cold bias in the FG surface temperature can explain the mean observed FG-departures in channels 4 to 6 at night-time for the selected region, whereas a 1.5 K warm bias is sufficient to explain the observed bias at day-time. Night-time biases of 5-10 K can similarly explain the observed pattern for other desert regions in Africa and Arabia (not shown). In other words, our

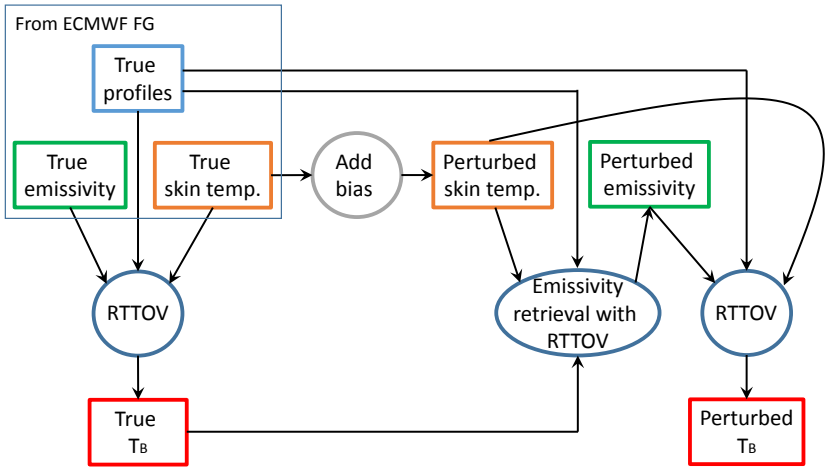

Figure 18: Flow-chart illustrating the simulation framework used in section 5.1. All RTTOV calculations refer to clear-sky calculation using the specular assumption. In section 5.2, the same framework is used, but the RTTOV calculations to produce the "true" T_B (and only these) employ the simple approximation of the Lambertian effect available in RTTOV. Similarly, in section 5.3, RTTOV is replaced by RTTOV-SCAT to calculate the "true" cloudy T_B only.

analysis suggests that the diurnal cycle in the surface temperature estimates used in the radiative transfer simulations in the ECMWF assimilation system appears to be too large in desert regions - it should be significantly warmer at night-time and a little colder at day-time.

The origin of this relatively large diurnal bias is likely to be a combination of sub-surface contributions for the true surface radiation, together with deficiencies in the diurnal cycle of the model surface temperature. In the ECMWF system, the surface contribution in the radiative transfer calculations is determined through the model skin temperature, representing temperature in the top-most millimetre of the land surface. However in arid regions, the penetration depth at microwave frequencies can be significant, reaching several centimetres at 50 GHz frequencies, as previously inferred by Prigent et al. (1999) or modelled by Grody and Weng (2008) and others. Sub-surface soil temperatures will exhibit a more dampened diurnal cycle, as is, for instance, captured by the ECMWF soil model for this area (Fig. 20). The deeper layers exhibit several K differences in amplitudes of the diurnal cycles. The night-time desert biases in the AMSU-A departures could be significantly reduced if we used a temperature taken from the top 10-30 cm of the ECMWF soil model to specify the surface contributions, instead of the skin temperature. The required penetration depth for these channels around 50 GHz is in good agreement with values derived by Galantowicz et al. (2011), albeit a little larger than values proposed by Prigent et al. (1999) or Grody and Weng (2008). The geographical regions affected by suspiciously large differences in emissivities between night and day (Fig. 17) are also similar to those highlighted by Norouzi et al. (2012) in similar studies of retrieved emissivity estimates that have been attributed to similar effects (their Figure 1). Alternative explanations for similar effects have been considered and discarded by Galantowicz et al. (2011). There are hence strong indications that penetration effects are at least partially explaining the observed biases also in our case.

Taking the penetration depth better into account would, however, introduce much larger negative biases during day-time, for which biases were previously small, so this explanation is not sufficient. A plausible hypothesis is that during day-time, the over-estimation of the effective surface temperature arising from

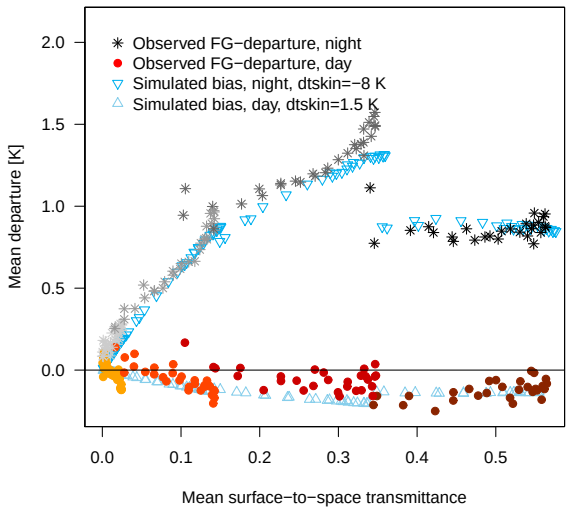

Figure 19: Effect of skin-temperature biases on observation departures: Stars and dots show mean FG-departures after bias correction in channels 4 to 7 of ATMS on S-NPP (channels 5-7 of ATMS are equivalent to channels 4-6 of AMSU-A). Statistics were accumulated by scan-position, and are plotted as a function of the mean surface-to-space transmittance. Stars show statistics accumulated for night-time over-passes (1:30 LT), and dots statistics for day-time over-passes (13:30 LT). Different shades of grey/red distinguish the different channels, with channel 4 displayed by the darkest grey/red. Statistics are based on all observations during the period June to August 2014, calculated from the **Base+seaice+land** *experiment, over a region in the Eastern Sahara as in Fig. 15. Also shown are results from simulations of the effect of skin temperature biases on the emissivity retrieval and the subsequent radiative transfer calculations (blue triangles), simulating an 8 K under-estimation of the skin temperature during night-time and a 1.5 K over-estimation during day-time. Note that channel 4 and 5 of ATMS are presently not assimilated in the ECMWF system. See main text for further details.*

the effects of penetration depth are - at least partially - compensated for by biases of the opposite sign in the modelling of the diurnal cycle of the skin temperature in the IFS. Supporting this, Trigo et al. (2015) found that the day-time peak of the skin temperature is under-estimated over desert regions by several K, whereas night-time values are more adequate (albeit slightly over-estimated). The two opposing biases may be the reason why day-time biases for the microwave data are smaller than night-time biases. Further work is required to confirm these explanations.

The previous analysis has been repeated for the 183 GHz sounding observations, used in the all-sky system. While the surface emissivities retrieved with the 89 GHz channel show similar diurnal bias pattern as the 50 GHz ones (albeit with slightly smaller amplitude of 0.03), the diurnal bias pattern for the departures in the 183 GHz sounding channels are much less clear. The reasons for this are not fully understood, but it may be a result of smaller surface penetration depths at 183 GHz and therefore a smaller effect, or it may be a reflection that larger uncertainties in the FG humidity fields dominate the statistics in these regions.

Our analysis suggests that the assimilation of 50 GHz microwave temperature sounding observations over desert regions is significantly hampered by large diurnal biases in the surface temperature used in the emissivity retrieval and radiative transfer calculations. The use of a more appropriate surface temperature estimate that reflects the deeper penetration depth over these surfaces is likely to offer some improvements in these regions. This could be derived using information from the soil model available in the IFS, following approaches of Prigent et al. (1999) or Galantowicz et al. (2011), allowing for different

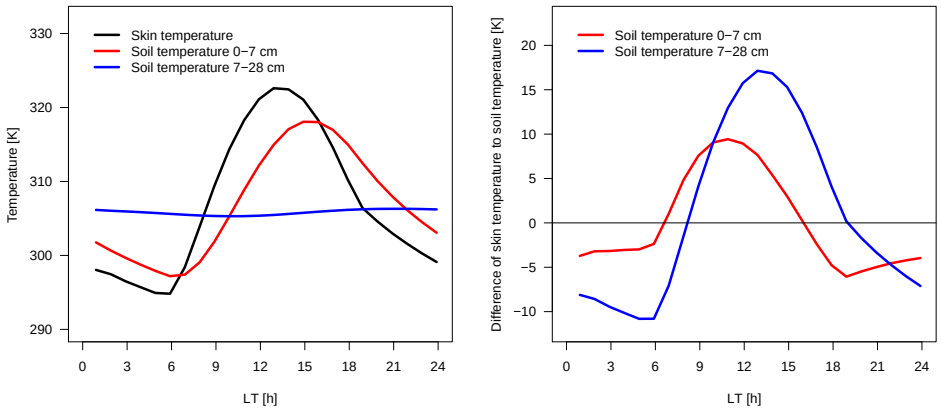

Figure 20: Left: Mean diurnal cycle of the model skin temperature (black), and the temperatures of the first (red) and second (blue) soil layer, taken from 0-11 h forecasts of the ECMWF operational high-resolution system for the period June-August 2016 over a region in the Eastern Sahara as in Fig. 15. Right: Diurnal cycle of the difference between the skin temperature and the temperature of the first (red) and second (blue) soil layer.

penetration depths for different frequencies. Alternatively, the simultaneous retrieval of a surface temperature and surface emissivity might be advantageous, as it would improve over the current situation where errors in the surface temperature are aliased into emissivity errors which subsequently prevent a reliable retrieval of the surface temperature in the 4DVAR sink variable. The simultaneous emissivity and skin temperature retrieval may require the use of several window channels to better separate the emissivity and surface temperature signal, in conjunction with appropriate background constraints on emissivity and surface temperature reflecting their expected errors over desert regions. Related approaches have, for instance, been developed by Boukabara et al. (2013) and others, and such concepts could be applied either prior or during 4DVAR (e.g., Pavelin and Candy 2014).

5.2 Snow

As highlighted before, snow-covered surfaces can show relatively large temporal, spatial and spectral variability in the estimated surface emissivity (e.g., Fig. 14), and they show larger numbers of rejected observations. For AMSU-A, the data are primarily rejected because channel 4 shows larger positive departures above the 0.7 K threshold applied to this window channel. An example of typical mean departure statistics for all data during January to March 2015 for the same region is shown in Fig. 21 (see Fig. 12 for the location). Relatively large positive departures are also present in the assimilated channels 5 and 6, and some channels also exhibit a weak diurnal cycle. Cloud effects have been found to be negligible during this period in this area, so the rejections are due to other inconsistencies between observations and FG equivalents. Of course, in the sample of assimilated observations the biases are much smaller, but as seen in Fig. 13b, a positive bias is still present in some snow-covered areas for the assimilated observations from channel 5.

A plausible source for these fairly large positive biases is the specular assumption used in the underlying radiative transfer calculations, both for the emissivity retrieval and the calculation of observation equivalents. Several authors have argued that snow behaves more like a Lambertian surface, and that assuming specular reflection instead leads to biases in the retrieved emissivities (e.g., Guedj et al 2010, Mätzler 2005). To investigate this aspect, stars and filled circles in Fig. 22 show mean departures for ATMS channels 4-7 from S-NPP for two regions with snow cover during January-March 2015, displayed in a similar

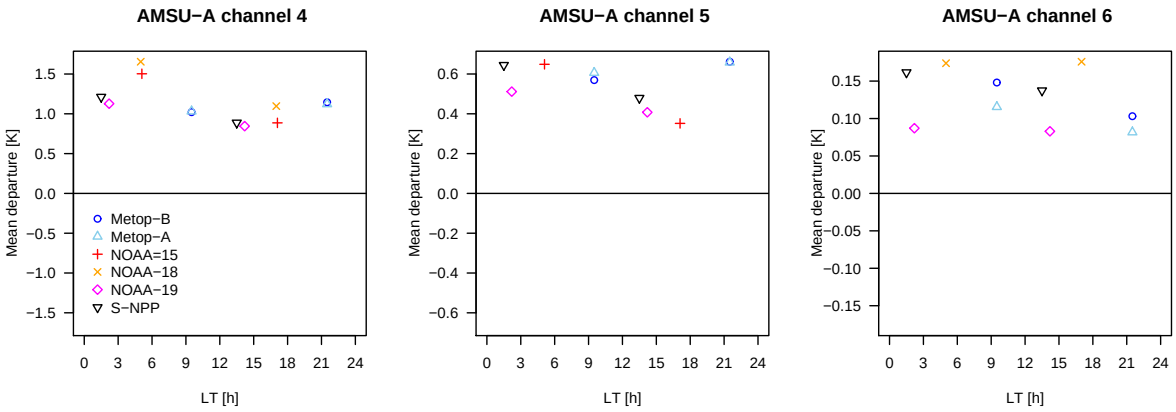

Figure 21: Mean FG departures after bias correction in AMSU-A channel 4 (left), channel 5 (middle) and channel 6 (right) as a function of the local solar time associated with the satellite over-pass for all observations with a zenith angle of less than 20 ° over a 2°×2° area centred around 62N 132E in Eastern Russia. The period is January to March 2016 and the statistics are taken from the ECMWF operational assimilation system. Also included are departures for equivalent ATMS channels flown on S-NPP (channels 5 to 7, respectively).

way as in Fig. 19 (see Fig. 12 for the locations). The statistics are taken from the clear-sky assimilation of ATMS. Each channel is indicated through different colour shades, and each datum represents the bias for a particular scan position. This means the variation with mean surface-to-space transmittance is caused primarily through different zenith angles, and within each channel the smallest surface-to-space transmittances will originate from the outer fields of views with the largest zenith angles (≈65°), whereas the largest surface-to-space transmittances are associated with the nadir views. For each channel the bias increases markedly with surface-to-space transmittance (ie, with decreasing zenith angle). But there is a noticeable drop in bias as a function of surface-to-space transmittance when we move from one channel to the next, quite different from the smooth behaviour previously seen in the desert case (Fig. 19) for which the bias could be explained through biases in the contribution from the surface temperature used.

Also shown in Fig. 22 are results from simulations of the Lambertian effect (blue triangles), obtained using a similar simulation framework as for the skin-temperature effect in the desert case (and again limited to clear-sky radiative transfer, see also Fig. 18). The simulations use atmospheric profiles and retrieved surface emissivities from the ECMWF system, extracted at S-NPP ATMS locations over a 48 h period in February 2015, to simulate "true" observations under the assumption of Lambertian behaviour. To simulate Lambertian surface scattering, the approximation available in RTTOV is used. This calculates the down-welling radiation simply by using an effective zenith angle of 55° for all channels, based on an approximation introduced by Mätzler (1987) that assumes horizontal homogeneity. Note, however, that this approximation is appropriate for zenith opacities of around 0.15-0.3 (surface-to-space transmittances of around 0.7-0.9, as encountered, for instance, for channel 3 of ATMS/AMSU-A). A lower effective zenith angle would be more appropriate for channels with larger zenith opacities, but this effect is neglected, hence we may over-estimate Lambertian effects for sounding channels at nadir. The simulated observations are then used to derive surface emissivities from channel 3, assuming specular reflection, and the resulting emissivity is used in subsequent radiative transfer simulations for the sounding channels, again assuming specular reflection. Radiative transfer terms in these calculations are always determined using the "true" atmospheric profiles. The difference between the simulated "true" observations and the specular simulations with the retrieved emissivities is shown as blue triangles in Fig. 22.

The simulated differences show a behaviour qualitatively very similar to the biases seen in the observa-

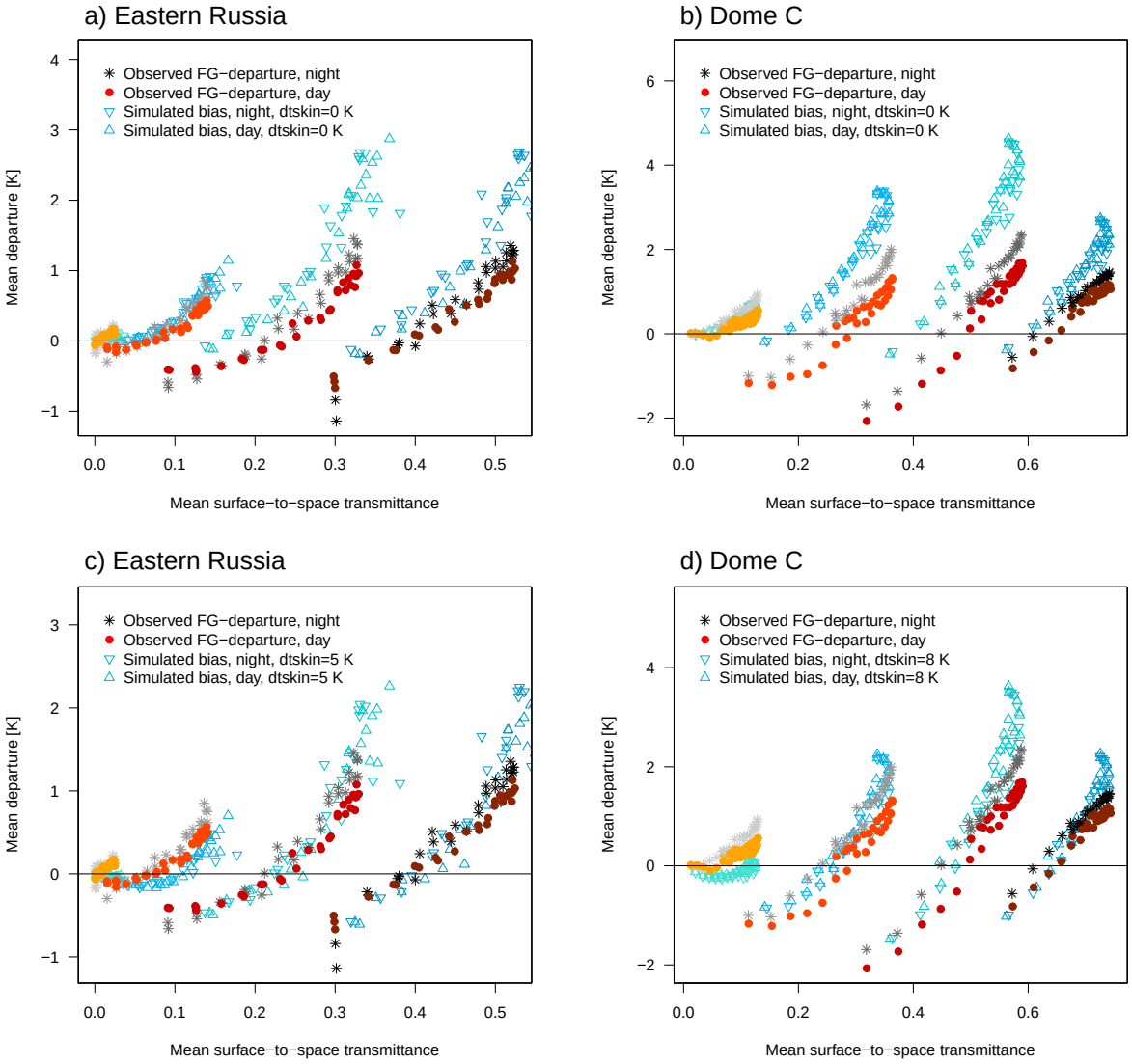

Figure 22: Lambertian and skin-temperature bias effects in observation departure statistics: Stars and dots show mean FG-departures after bias correction in channels 4 to 7 of ATMS on S-NPP for a region in Eastern Russia (a, c) and Dome C (b, d), similar to Fig. 19, but for January to March 2015. Also shown are results from simulations of the biases arising from neglecting Lambertian effects in the emissivity retrieval and subsequent forward calculations (blue triangles, panels a and b). Simulation statistics shown in panels c and d additionally include simulation of the effect of a 5 and 8 K bias in the skin temperature used in the emissivity retrieval and the subsequent radiative transfer calculations (blue triangles). Note that channel 4 and 5 of ATMS are presently not assimilated in the ECMWF system. Note that for Dome C the day/night distinction is less meaningful for large parts of the period. See main text for further details.

tions: for each channel, the differences are relatively small for the smallest surface-to-space transmittances, for which zenith angles are close to 55° and the Lambertian effect is small, and then increase significantly with surface-to-space transmittance, ie for observations with zenith angles approaching 0° for which the Lambertian effect is largest. Guedj et al (2010) and Mätzler and Rosenkranz (2007) have similarly found the Lambertian assumption to be a good approximation around Dome C for AMSU-A observations, albeit for winter cases. There is, however, a remaining offset between observed biases and

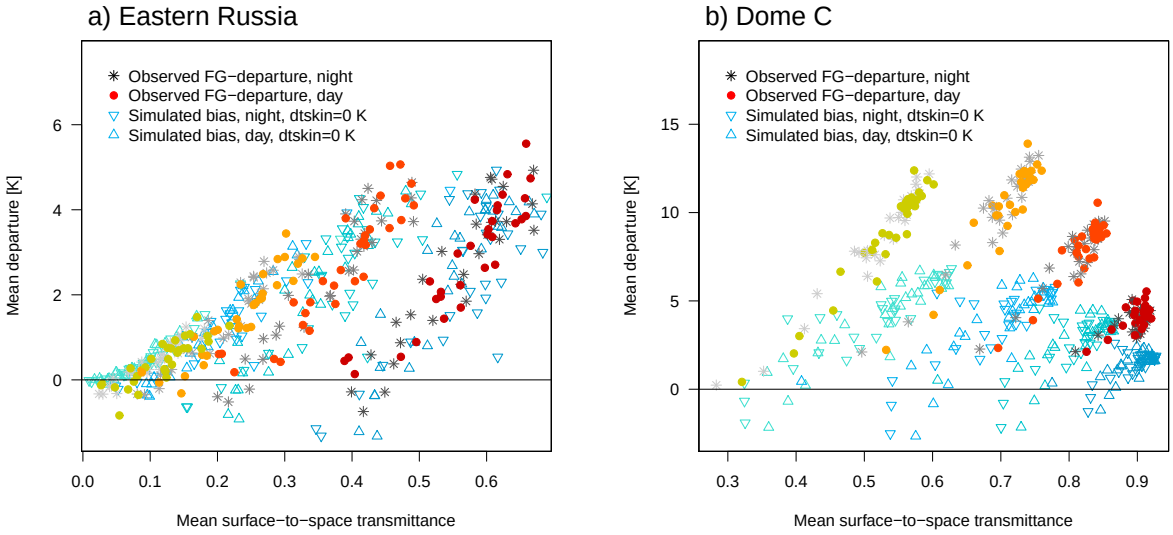

Figure 23: As Fig. 22a, b, but for the 183 GHz ATMS channels 18 to 21. To obtain these departure statistics, the emissivity retrieval is performed using channel 17, equivalent to the approach taken for MHS. Note that none of these channels from ATMS are presently assimilated over snow.

the simulations in Fig. 22a, b. Some of this is likely due to using a fixed effective zenith angle in the approximation used to simulate Lambertian effects. At least for channels 4-6, the offset can be explained by a positive bias in the skin temperature in addition to the Lambertian effects (Fig. 22c and d).

Departures for the surface-sensitive humidity-sounding channels of ATMS similarly show characteristics that could be explained by neglecting diffuse surface reflection effects (e.g., Fig. 23). The effect appears to be even stronger, but there is also significantly more scatter in the statistics. The example for Eastern Russia shows good agreement between the observed biases and the simulations with the simple Lambertian parameterisation even in the absence of a skin-temperature bias (Fig. 23a), though additional simulations suggest that skin-temperature biases of a few degrees cannot be ruled out. In contrast, while observed biases for the Dome C example also exhibit pattern typical for a diffuse surface behaviour, the biases appear to be much stronger than what could be explained by the simple Lambertian approximation alone. Additional effects appear to play a role, but the mechanism is not fully clear. The biases could be explained by a severe under-estimation of the skin temperature, in contrast to the finding in Fig. 22d, or may be the result of other biases in the observations or the model fields. Note, however, that this example shows extreme surface-sensitivity for the displayed channels in this region, resulting from a combination of high orography and an extremely dry atmosphere, making any extraction of information on the atmosphere particularly challenging. The presented results are based on the clear-sky use of ATMS, but cloud effects do not play a significant role over both areas during this period, so results will be applicable to the all-sky treatment of, say, MHS as well.

Figure 24 shows where the behaviour seen in the departures in Fig. 22 is particularly prominent for the January to March 2015 period. The Figure shows the difference between the bias corrected departures of ATMS channel 5 at low zenith angles and those of channel 4 at high zenith angles. That is, it measures the size of the discontinuity that is apparent when moving from one channel to the next in the graphs of the observed mean departures as a function of the surface-to-space transmittance. The map shows that the effect is primarily confined to snow-covered surfaces, but is also present over sea-ice regions. While not discussed in greater detail here, some sea-ice regions indeed exhibit behaviour that is very similar to

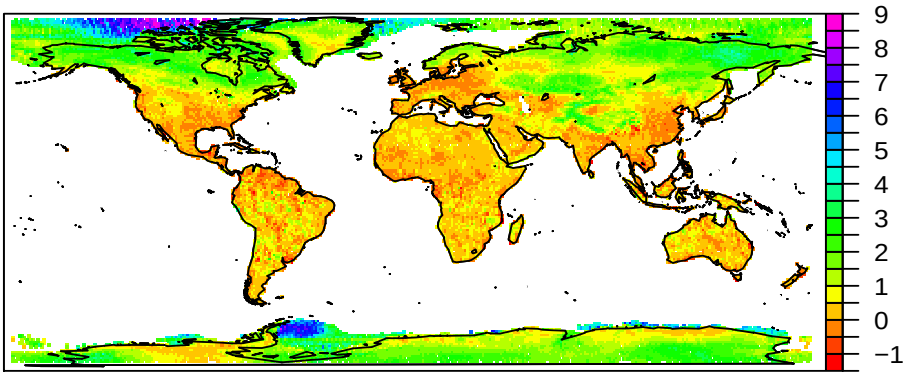

Figure 24: Difference in the observed mean departure (after bias correction) in S-NPP ATMS channel 5 for zenith angles below 10° and the observed mean departure in channel 4 at zenith angles greater than 50°, averaged over the period January-March 2015. Statistics are for data before quality control, taken from the **Base+seaice+land** *experiment.*

that of snow-covered land surfaces, with some signs of Lambertian behaviour. This is very likely linked to the departure biases over sea-ice as well as the changes to the mean temperature and humidity analyses noted earlier in the context of the OSE with the observations over sea-ice.

The above analysis suggests benefits from using a Lambertian approximation over snow-covered surfaces, and this could be investigated further in the IFS. Partial Lambertian approximations could also be considered, as suggested by, for instance, Rosenkranz and Mätzler (2008) or Guedj et al (2010). However, it is also apparent that some biases may originate from biases in the surface temperature used, and estimating the appropriate degree of Lambertianity as well as surface temperature biases may be difficult. As motivated in Fig. 22 and Fig. 23, using observations from different channels and different viewing geometries may offer some scope to adequately separate these aspects. The relatively simple Lambertian concept considered here should give benefits for some of the already assimilated sounding channels over snow and sea-ice, but may also enable the assimilation of the lower humidity sounding channels (e.g., 18 and 19 of ATMS or 5 of MHS) that are presently not used over snow-covered (or sea-ice) surfaces, at least in some regions. However, the Dome C example suggests that there may also be other aspects to consider. Note, in this context, that Baordo and Geer (2015) also found unexplained bias pattern over sea-ice for 183 GHz channels from the conically-scanning SSMIS, in terms of departure statistics and in terms of a systematic difference in the retrieved emissivties at 150 GHz and 183 GHz. These features will not be addressed by the simple implementation of Mätzler's (1987) approximation of the Lambertian effect used in RTTOV, as it uses a fixed effective zenith angle of 55° to estimate the reflected downwelling radiation, very close to SSMIS's zenith angle of 53°. However, this simple implementation neglects the dependence of this effective angle on the channel optical depth, and further work is needed to investigate the effect of this approximation. Further improvements may require explicit modelling of snow emission and reflection using a snow radiative transfer model (see, e.g., Royer et al. 2017) with information from the snow model able to describe multi-layer snow situations.

5.3 Cloud signals in clear-sky assimilation

Cloud signals pose an additional general issue for the dynamic emissivity retrieval underlying the assimilation of surface-sensitive microwave data: cloud signals can alias into the retrieved emissivity (e.g.,

Tiang et al. 2014). In the clear-sky system at ECMWF, we retrieve surface emissivities from channel 3 observations using an equation that is based on clear-sky radiative transfer. If the channel 3 observations are affected by clouds this will mean that the retrieved emissivity will be in error, as the cloud signal is mis-interpreted as an emissivity signal. In the all-sky framework, in which the emissivity retrieval is performed based on an all-sky radiative transfer, similar aliasing can occur in places where observed and model clouds do no match, as analysed in some detail by Baordo and Geer (2016).

In the following, we will highlight the effect of clouds on the emissivity estimation in the clear-sky assimilation of AMSU-A observations in more detail using a simulation framework, similar to the one used in the previous sub-sections. To do so, we use simulations of cloudy and clear AMSU-A observations, obtained over a 48 h period between 30 June 2015 21Z and 2 July 21 Z. These were calculated with RTTOV-SCATT from atmospheric profiles and skin-temperature information generated with the ECMWF assimilation system over the period in question, as described previously. We can now use the simulated cloudy channel 3 observations to retrieve the surface emissivity, applying the usual methods assuming clear-sky radiative transfer (Karbou et al. 2006), and then compare the result back to the "true" surface emissivities used to obtain the simulated cloudy observations.

The difference between the retrieved and the "true" surface emissivity values is shown in Fig. 25 for a 12-hour period. As can be seen, while the difference is small for many regions, there are also some places for which very sizeable differences are found, even reaching 0.05 in places. The latter are the regions for which the channel 3 observations are significantly affected by clouds or precipitation. The emissivity differences illustrate the error that results from using observations that are cloud-affected in the emissivity retrieval scheme that assumes clear-sky conditions. The effect is sufficient to explain some short-term variations in emissivity previously noted in the context of Fig. 14.

If observations that are significantly cloud-affected were to be identified and rejected the error illustrated in Fig. 25 would of course not matter. However, as we will see in the following, the error does affect

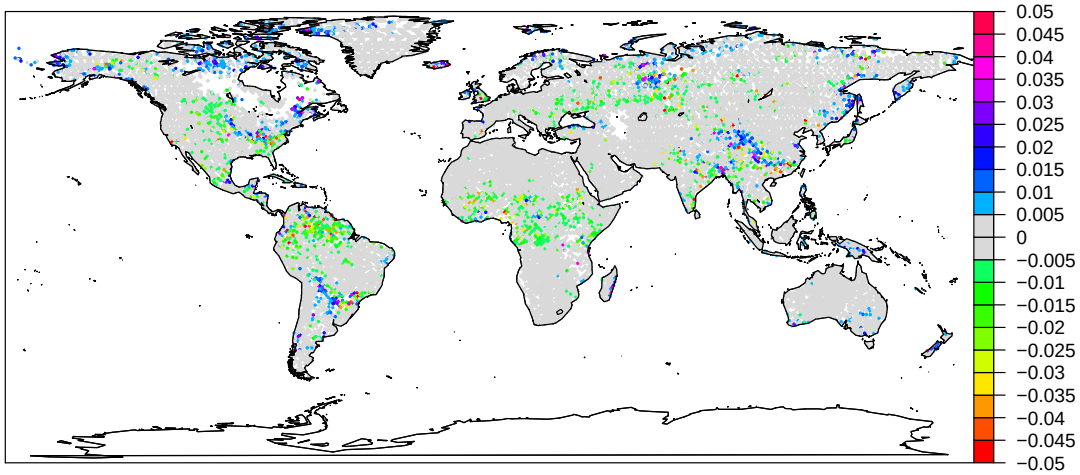

Figure 25: Effect of cloud contamination on the emissivity retrieval: Difference between retrieved and "true" emissivities from simulations in which the retrieved emissivities are calculated from simulated cloud-affected observations in AMSU-A channel 3 based on a clear-sky radiative transfer equation. Simulations are based on atmospheric conditions covering the period 2 July 2015 9-21Z. See main text for further details on the simulations.

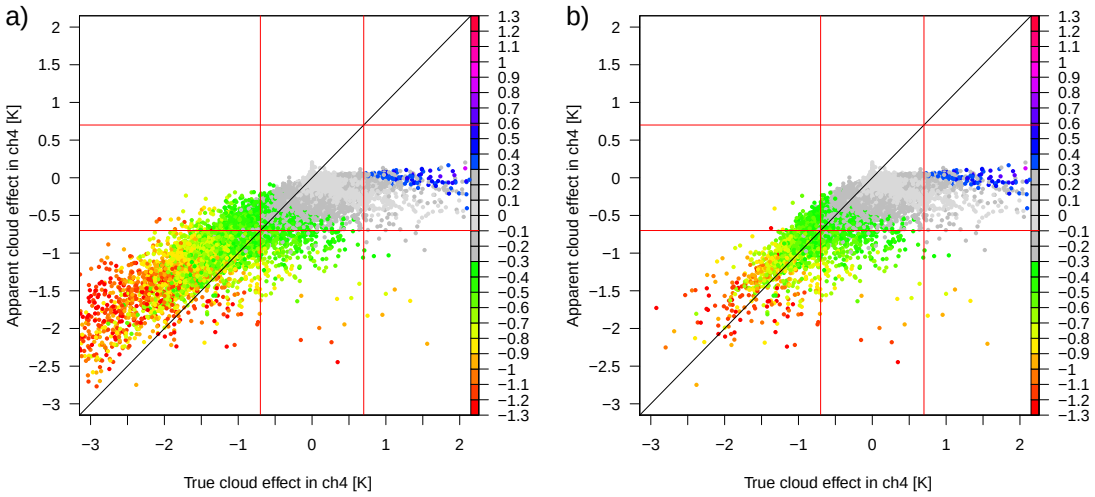

Figure 26: a) Scatter plot of the "true" cloud effect in AMSU-A channel 4 [K] versus the apparent cloud effect [K]. The cloud effect is the difference between cloudy and clear-sky simulations. For the calculations of the "true" cloud effect, the same emissivities are used in both simulations, whereas for the apparent cloud effect emissivities for the clear-sky simulations have been retrieved from simulated cloud-affected observations in AMSU-A channel 3 based on a clear-sky radiative transfer equation. Colour coding also indicates the true cloud effect for channel 5 simulations. Simulations are based on atmospheric conditions covering the period 30 June 2015 21Z to 2 July 21Z. See main text for further details on the simulations. b) As a), but showing only samples for which the difference in the simulated cloudy brightness temperatures in channel 1 and 15 is less than 3 K, adapted from the observation-based cloud screening applied in assimilation.

one of the methods used to screen for clouds, leading to observations that are significantly cloud affected to be assimilated. The main criterion to identify cloud-affected observations is a check on the absolute value of the background departure in channel 4: a significant difference between the observations and the clear-sky equivalents in this window channel is taken as indicative of clouds or precipitation. A threshold of 0.7 K is used for this purpose. To obtain the channel 4 departure, the retrieved emissivity with the erroneous cloud signal is used. The cloud signal that has been aliased into the emissivity retrieval will hence affect the clear-sky simulations for channel 4, leading to an error that is similar to a cloud signal. Note that additional cloud screening is performed based on detecing a scattering signal in the difference between 23 GHz and 89 GHz observations, and this check is unaffected.

We have simulated the effect on the channel 4 departure using the framework introduced earlier, and the results are summarised in Fig. 26a. The "apparent cloud effect in channel 4" is the difference between the "true" cloudy observation and the clear-sky simulation that uses the erroneous retrieved surface emissivity, and in the absence of other errors the latter would form the basis of cloud detection in the present clear-sky system. It is clear that the apparent cloud effect is considerably suppressed compared to the "true cloud effect" ie the difference between the true cloudy and true clear-sky simulations. The largest cloud effects in channel 4 arise from scattering, leading to a reduction in the simulated cloudy brightness temperatures of up to several tens of K (cropped in Fig. 26 to focus on more subtle cloud signals). If we take 0.7 K as a crude measure of indicating a significant cloud effect a number of observations for which the true cloud effect would be considered "significant" (e.g., outside the red lines in Fig. 26a) would not be flagged as cloudy if we instead base our decision on the apparent cloud effect. In reality, the channel 4 departure check is of course also affected by instrument noise and background errors. Nevertheless, the number of observations passing the channel 4 departure check is sometimes used as an indicator of a superior emissivity specification (e.g., Karbou et al. 2006), and it is clear from this analysis that this

interpretation can be very misleading in the case of the dynamically retrieved emissivities.

While the channel 4 departure check is the most active in our assimilation experiments, an additional cloud check is performed that uses the difference of the observed brightness temperatures in channel 1 and 15 and is hence independent of the retrieved emissivities. Fig. 26b shows the same simulations as discussed above, but displaying only the sample that is not screened out by this additional check. While the additional check removes the observations with the largest true cloud effect, the smaller apparent cloud effect in channel 4 due to the retrieved emissivities will still lead to unreliable rejections.

Also shown in Fig. 26 is the cloud contamination in channel 5, ie the lowest assimilated sounding channel. Many channel 5 observations that show an apparent cloud effect in channel 4 between ± 0.7 K suffer from very significant cloud contamination, including after the scatter index check has been applied (Fig. 26b). At the same time, also observations for which the true cloud effect in channel 4 is between ± 0.7 K suffer from very significant cloud contamination in channel 5. Either way, this is likely to affect the extraction of temperature information during the assimilation of this channel. The propagation of the effect of residual cloud contamination into the atmospheric analysis could be simulated further, but this is considered beyond the scope of the present study.

The present analysis highlights that cloud detection and cloud contamination are problematic in some situations in the present assimilation approach. It may be beneficial to tighten the presently used check on the scatter index or to develop further alternative cloud detection methods that do not rely on background departures to increase the robustness of the cloud detection for the clear-sky assimilation. Alternatively, all-sky assimilation for these channels would avoid the need for cloud detection.

6 Conclusions and outlook

This memorandum assessed the current use of surface-sensitive microwave radiances over land and sea-ice in the ECMWF assimilation system. The main findings are:

- Surface-sensitive microwave radiances over land and sea-ice have a significant positive forecast impact in the ECMWF system (2-3 % reduction in forecast error for the 500 hPa geopotential over the extra-tropics). When added incrementally to an otherwise full observing system, observations over sea-ice, humidity-sounding radiances over land, and temperature-sounding radiances over land all contribute significantly to this positive forecast impact. The impact of the observations over land is strongest over the Northern Hemisphere, whereas the data over sea-ice during winter give the largest contributions over the Southern Hemisphere. Little impact is observed in the tropical region.

- The size of the forecast impact shows some seasonal dependence, related to, for instance, the presence of sea-ice as expected. For the Northern Hemisphere, the impact of the data over land is smaller during winter, most likely related to a more restricted and less optimal use of the observations over snow.

- Adjoint diagnostics support the hypothesis that the largest impact from the land/sea-ice data originates from remote areas not well-covered by conventional observations.

- An analysis of data usage and departure statistics suggests that the current method of retrieving surface emissivity from window channels has deficiencies particularly in the following areas:

Deserts: most likely due to biases in the temperature used to specify surface radiation, likely arising from a combination of penetration effects and diurnal model biases.

Snow: most likely primarily due to assuming specular reflection in the emissivity retrieval and the subsequent radiative transfer calculations, possibly combined with some biases in skin temperature.

Clouds: cloud signals are erroneously aliased into the retrieved surface emissivities. This also affects the presently used cloud detection in the clear-sky system.

- The quality control currently applied is mostly successful in protecting the analysis from the deficiencies identified over desert and snow surfaces.

The present study provides a clear confirmation of the benefit of assimilating surface-sensitive microwave sounding data over land and sea-ice. A number of incremental improvements have contributed to this impact, including a gradual increase in the number of observations assimilated, both in terms of the number of channels assimilated, but also the number of instruments, as well as refinements in the emissivity estimation and assimilation choices. While the impact of each of these enhancements has mostly been small, it is clear that the combination of these developments now underpins a clear benefit of this data. This is true for the overall impact, but also in terms of the individual impact from data over sea-ice, humidity sounding, and temperature sounding data, respectively. The study has also highlighted some inconsistencies in the use of surface-sensitive microwave data, with equivalent channels being used in some areas for one instrument, but not another, and our results give further incentive to harmonise these aspects and further expand the use of this data. Such harmonisation has been performed in cycle 43r3, together with the activation of 118 GHz channels from MWHS-2 over land (Weston et al. 2017).

This memorandum has also highlighted areas with scope for improvements in specific geographical areas, namely desert and snow areas, where the current use is prone to significant biases. Current quality control procedures appear to be adequate in protecting the analysis from these biases, but it is nevertheless desirable to improve the data usage in these regions. To address these issues will require adjustments to the dynamic emissivity method, either involving the derivation of additional surface properties (e.g., penetration depth or effective surface temperature in the desert case, or Lambertian parameter and effective surface temperature in the snow case, following concepts proposed by Guedj et al. 2010, Galantowicz et al. 2011) or different modelling or assimilation approaches.

While the dynamic emissivity method provides a framework to adequately treat surface emissivity for most other surfaces, it is also clear that there are also short-comings of the method in general. Two of these have been illustrated in this work, that is, the aliasing of cloud information into the emissivity retrieval in the clear-sky framework, and the influence of errors in the model skin temperature used in the emissivity retrieval. Other sources of error, not covered here, are errors in the atmospheric model background fields used for the emissivity retrieval which Karbou et al. (2006) estimates to be typically less than 1 %. The general uncertainties have been highlighted before in similar context by other authors (e.g., Tian et al. 2014, Baordo and Geer 2016). It is clear that the simple separate retrieval of emissivity from a single window channel prior to the assimilation is particularly prone to aliasing of uncertainties into the emissivity retrieval.

The above considerations suggest that further progress in the assimilation of surface-sensitive channels over land and sea-ice in the ECMWF system will require considerable revision of the methods used to specify surface emissivity and skin temperature. Different approaches with different levels of sophistication could be considered:

Accounting for the penetration depth in desert regions: The diurnal biases in desert regions could be

improved by taking the penetration depth into account and using data from the soil model. While this appears attractive, as it would make better use of the model information available, it is also likely that it will not solve all bias problems, as discussed in section 5.1.

Simultaneous retrieval of skin temperature and emissivity: Presently, emissivity and skin temperature are retrieved sequentially, the emissivity prior to the assimilation, the skin temperature during 4DVAR, aggravating the aliasing of errors. Instead, both could be retrieved simultaneously, either prior to the assimilation or within 4DVAR. This would require the use of several window channels with different surface-sensitivity to allow the separation of the skin temperature and emissivity signal. The approach should give some benefit, for instance, in the desert case. However, as some of the issues highlighted in this memorandum are due to biases in the model skin temperature used rather than random errors, the chosen approach should be capable of dealing with these model skin temperature biases (regardless of the penetration depth issues over deserts). A retrieval prior to the assimilation may be more advantageous for this.

Retrieval of free parameters of an emissivity parameterisation: Presently, the emissivity retrieval is done separately for each field of view, with no prior information, no constraint between different frequencies, and no link between different sensors. This could be evolved into an approach that includes a background emissivity, and allows a slow evolution of the surface emissivity from cycle to cycle, for instance by updating a suitable parameterisation of the surface emissivity. Concepts in this direction have been proposed and investigated before, based on an external Kalman Filter framework (Krzeminski et al. 2009, Bormann 2014). This could be developed further, and updating of the variables of the emissivity parameterisation, combining several sensors, could even be included as an exuilliary control variable in 4DVAR. Other useful variables could be included as well, for instance a Lambertianity parameter, or parameters relating to sea-ice.

Towards coupled physical approaches: Initially, the emissivity and further surface parameters could be kept independent of the surface models of the IFS and simply propagated from one assimilation cycle to the next using persistence. Longer-term, links with the surface models could be explored, opening possibilities to influence the surface analysis in coupled assimilation approaches. Physical modelling of the surface-related radiative transfer aspects could be considered in some areas. This may be particularly advantageous in regions with considerable temporal changes, such as snow-covered areas, and snow radiative transfer models could be included (e.g., Royer et al. 2017). Ultimately, these approaches could lead to benefits in terms of better constraining aspects of the land surface analysis, by directly using passive microwave radiances. This is likely to remain a long-term aim for some time and will rely on developments in coupled data assimilation, but possibilities in this direction could at least be explored.

The above options provide a longer-term framework for future developments, and further work is required to identify the most practical and promising approach and what level of sophistication is needed. However, it is clear that there is potential for obtaining additional information from the observations, not least on surface conditions, and this is likely to be a promising longer-term perspective.

References

Baordo, F., and A. Geer, 2015: Microwave surface emissivity over sea-ice. NWP-SAF Visiting Scientist report NWP-SAF-VS-026, ECMWF, available from https://nwpsaf.eu/publications/vs_reports/nwpsaf–ec–vs–026.pdf.

Baordo, F., and A. Geer, 2016: Assimilation of SSMIS humidity-sounding channels in all-sky conditions over land using a dynamic emissivity retrieval. *Q. J. R. Meteorol. Soc.*, **142**, 10.1002/qj.2873.

Bechtold, P., N. Semane, P. Lopez, J.-P. Chaboureau, A. Beljaars, and N. Bormann, 2014: Representing equilibrium and nonequilibrium convection in large-scale models. *J. Atmos. Sci.*, **71**, 734–753.

Bormann, N., 2014: Reformulation of the emissivity Kalman Filter atlas. Research Department Memorandum RD14-190, available from http://intra.ecmwf.int/publications/library/do/references/show?id=1471, ECMWF, Reading, UK.

Boukabara, S.-A., K. Garrett, C. Grassotti, F. Iturbide-Sanchez, W. Chen, Z. Jiang, S. Clough, X. Zhan, P. L. ad Q. Liu, T. Islam, V. Zubko, and A. Mims, 2013: A physical approach for a simultaneous retrieval of sounding, surface, hydrometeor, and cryospheric parameters from SNPP/ATMS. *J. Geophys. Res.*, **118**, 12,600–12,619, doi:10.1002/2013JD020448.

Cardinali, C., 2009: Monitoring of the observation impact on the short-range forecast. *Q. J. R. Meteorol. Soc.*, **135**, 239–250.

Cardinali, C., 2014: Observation impact on the short-range forecast. In Advanced Data Assimilation for Geosciences: Lecture Notes of the Les Houches School of Physics: Special Issue, June 2012, OUP Oxford, 165–180, DOI:10.1093/acprof:oso/9780198723844.003.0006.

Cardinali, C., and F. Prates, 2009: Forecast sensitivity to observations (FSO) as a diagnostic tool: monitroing the impact of observations of the short range forecast. In Proceedings of the ECMWF workshop on diagnostics of data assimilation system performance, ECMWF, 117–132.

Chambon, P., and A. Geer, 2017: All-sky assimilation of Megha-Tropiques/SAPHIR radiances in the ECMWF numerical weather prediction system. Technical Memorandum 802, ECMWF, Reading, UK, 45 pp.

Dee, D., 2004: Variational bias correction of radiance data in the ECMWF system. In ECMWF Workshop on Assimilation of High Spectral Resolution Sounders in NWP, ECMWF, Reading, UK, 97–112.

Di Tomaso, E., and N. Bormann, 2012: Assimilation of ATOVS radiances at ECMWF: second year EUMETSAT fellowship report. EUMETSAT/ECMWF Fellowship Programme Research Report 26, ECMWF, Reading, U.K., 27 pp.

Di Tomaso, E., N. Bormann, and S. English, 2013: Assimilation of ATOVS radiances at ECMWF: third year EUMETSAT fellowship report. EUMETSAT/ECMWF Fellowship Programme Research Report 29, ECMWF, Reading, U.K., 26 pp.

English, S., 2008: The importance of accurate skin temperature in assimilating radiances from satellite sounding instruments. *IEEE Trans. Geosci. Remote Sens.*, **46**, 403–408.

Galantowicz, J., J.-L. Moncet, P. Liang, A. Lipton, G. Uymin, C. Prigent, and C. Grassotti, 2011: Subsurface emission effects in AMSR-E measurements: Implications for land surface microwave emissivity retrieval. *J. Geophys. Res.*, **116**, D17105, doi:10.1029/2010JD015431.

Geer, A., F. Baordo, N. Bormann, and S. English, 2014: All-sky assimilation of microwave humidity sounders. Technical Memorandum 741, ECMWF, Reading, U.K., 57 pp.

Geer, A., F. Baordo, N. Bormann, S. English, M. Kazumori, H. Lawrence, P. Lean, K. Lonitz, and C. Lupu, 2017: The growing impact of satellite observations sensitive to humidity, cloud and precipitation. *Q. J. R. Meteorol. Soc.*, **143**, in reviw.

Grody, N., and F. Weng, 2008: Microwave emission and scattering from deserts: Theory compared with satellite measurements. *IEEE Trans. Geosci. Remote Sensing*, **46**, 361–375.

Guedj, S., F. Karbou, F. Rabier, and A. Bouchard, 2010: Toward a better modeling of surface emissivity to improve AMSU data assimilation over antarctica. *IEEE Trans. Geosci. Remote Sensing*, **4**, 1976–1985.

Karbou, F., E. Gérard, and F. Rabier, 2006: Microwave land emissivity and skin temperature for AMSU-A and -B assimilation over land. *Q. J. R. Meteorol. Soc.*, **132**, 2333–2355.

Kelly, G., and P. Bauer, 2008: Use of AMSU-A surface channels to obtain surface emissivity over land, snow and ice for Numerical Weather Prediction. In Proceedings of the 11th international TOVS study conference, Budapest, Hungary, CIMSS, University of Wisonsin, Madison, US, 167–179.

Krzeminski, B., N. Bormann, P. Bauer, and F. Karbou, 2009: Improved use of surface-sensitive microwave radiances at ECMWF. In Proceedings of the 2009 EUMETSAT Meteorological Satellite Conference, Bath, UK, EUMETSAT, Darmstadt, Germany, available from: http://www.eumetsat.int/website/wcm/idc/idcplg?IdcService=GET_FILE&dDocName=PDF_CONF_P55_S8_43_KRZEMINS_P&RevisionSelectionMethod=LatestReleased&Rendition=Web.

Krzeminski, B., N. Bormann, F. Karbou, and P. Bauer, 2008: Towards a better use of AMSU over land at ECMWF. In Proceedings of the 16th international TOVS study conference, Angra dos Reis, Brazil, CIMSS, University of Wisonsin, Madison, US, paper A26, available from http://cimss.ssec.wisc.edu/itwg/itsc/itsc16/proceedings/A26_Krzeminski_.pdf.

Langland, R., and N. Baker, 2004: Estimation of observation impact using the NRL atmospheric variational data assimilation adjoint system. *Tellus A*, **56(3)**, 189–201.

Lawrence, H., and N. Bormann, 2014: First year report: The impact of hirs on ecmwf forecasts, adding atms data over land and sea ice and new observation errors for amsu-a. EUMETSAT/ECMWF Fellowship Programme Research Report 34, ECMWF, Reading, U.K., 36 pp.

Lawrence, H., N. Bormann, and S. English, 2014: Scene-dependent observation errors for the assimilation of AMSU-A. EUMETSAT/ECMWF Fellowship Programme Research Report 39, ECMWF, Reading, U.K., 30 pp.

Liu, Q., F. Weng, and S. English, 2011: An improved fast microwave water emissivity model. *IEEE Trans. Geosci. Remote Sens.*, **49**, 1238–1250.

Lopez, P., 2014: Comparison of NCEP stage IV precipitation composites with ECMWF model. Technical Memorandum 728, ECMWF, Reading, UK.

Mätzler, C., 1987: Applications of the interaction of microwaves with the natural snow cover. *Remote Sens. Rev.*, **2**, 259–387.

Mätzler, C., 2005: On the determination of surface emissivity from satellite observations. *IEEE Geosci. Remote Sensing Letters*, **2**, 160–163.

Mätzler, C., and P. Rosenkranz, 2007: Dependence of microwave brightness temperature on bistatic surface scattering: Model functions and application to AMSU-A. *IEEE Trans. Geosci. Remote Sensing*, **45**, 2130–2138.

McNally, A., C. Lupu, C. Cardinali, A. Geer, R. Forbes, K. Lonitz, M. Diamantakis, and C. Peubey, 2014: Impact of satellite data on global NWP. In Presentation at the ECMWF Seminar 2014: Use of Satellite Observations in Numerical Weather Prediction, ECMWF, Reading, United Kingdom, http://www.ecmwf.int/sites/default/files/elibrary/2014/14686–impact–satellite–data–global–nwp.pdf.

Norouzi, H., W. Rossow, M. Temimi, C. Prigent, M. Azarderakhsh, S. Boukabara, and R. Khanbilvardi, 2012: Using microwave brightness temperature diurnal cycle to improve emissivity retrievals over land. *Remote Sensing of Environment*, **123**, 470–482.

Pavelin, E., and B. Candy, 2014: Assimilation of surfacesensitive infrared radiances over land: Estimation of land surface temperature and emissivity. *Q. J. R. Meteorol. Soc.*, **140**, 1198–1208.

Prigent, C., W. Rossow, E. Matthews, and B. Marticorena, 1999: Microwave radiometer signatures of different surface types in deserts. *J. Geophys. Res.*, **104**, 12,147–12,158, doi:10.1029/1999JD900153.

Rosenkranz, P., and C. Mätzler, 2008: Dependence of AMSU-A brightness temperatures on scattering from Antarctic firn and correlation with polarization of SSM/I data. *IEEE Geosci. Remote Sensing Letters*, **5**, 769–773.

Royer, A., A. Roy, B. Montpetit, O. Saint-Jean-Rondeau, G. Picard, L. Brucker, and A. Langlois, 2017: Comparison of commonly-used microwave radiative transfer model for snow remote sensing. *Remote Sensing of Environment*, **190**, 247–259.

Tian, Y., C. Peters-Lidard, K. Harrison, C. Prigent, H. Norouzi, F. Aires, S.-A. Boukabara, F. Furuzawa, and H. Masunaga, 2014: Quantifying uncertainties in land-surface microwave emissivity retrievals. *IEEE Trans. Geosci. Remote Sensing*, **52**, 829–840.

Trigo, I., S. Boussetta, P. Viterbo, G. Balsamo, A. Beljaars, and I. Sandu, 2015: Comparison of model land skin temperature with remotely sensed estimates and assessment of surface-atmosphere coupling. Technical Memorandum 774, ECMWF, Reading, UK.

Weston, P., N. Bormann, A. Geer, and H. Lawrence, 2017: Harmonisation of the usage of microwave sounder data over land, coasts, sea-ice and snow: First year report. EUMETSAT/ECMWF Fellowship Programme Research Report 45, ECMWF, Reading, U.K.